

A NEW CATALOG OF HOMOGENISED ABSORPTION LINE INDICES FOR MILKY WAY GLOBULAR CLUSTERS FROM HIGH-RESOLUTION INTEGRATED SPECTROSCOPY

Hak-Sub Kim^{1,2}, Jaeil Cho^{1,3}, Ray M. Sharples⁴, Alexandre Vazdekis^{5,6},
Michael A. Beasley^{5,6} and Suk-Jin Yoon^{2,7}

¹Co-first authors

²Center for Galaxy Evolution Research, Yonsei University, Seoul 03722, Republic of Korea

³Gwacheon National Science Museum, Gyeonggi 13817, Republic of Korea

⁴Department of Physics, University of Durham, South Road, Durham DH1 3LE, UK

⁵Instituto de Astrofísica de Canarias, La Laguna, E-38200 Tenerife, Spain

⁶Departamento de Astrofísica, Universidad de La Laguna, Spain

⁷Department of Astronomy, Yonsei University, Seoul 03722, Republic of Korea

`sjyoon0691@yonsei.ac.kr`

Received _____; accepted _____

Draft (November 26, 2021) to be submitted to ApJ Supplement

ABSTRACT

We perform integrated spectroscopy of 24 Galactic globular clusters. Spectra are observed from one core radius for each cluster with a high wavelength resolution of $\sim 2.0 \text{ \AA}$ FWHM. In combination with two existing data sets from Puzia et al. (2002) and Schiavon et al. (2005), we construct a large database of Lick spectral indices for a total of 53 Galactic globular clusters with a wide range of metallicities, $-2.4 \lesssim [\text{Fe}/\text{H}] \lesssim 0.1$, and various horizontal-branch morphologies. The empirical index-to-metallicity conversion relationships are provided for the 20 Lick indices for the use of deriving metallicities for remote, unresolved stellar systems.

Subject headings: globular clusters: general — catalogs — stars: abundances

1. INTRODUCTION

Globular clusters (GCs) are thought to have formed along with the bulk of stars in galaxies and thus contain crucial information on the formation histories of their host galaxies. The properties of GCs in external galaxies are derived by comparing their integrated light with Galactic globular clusters (GGCs). Furthermore, reliable databases for GGCs are crucial for validating and calibrating theoretical stellar population models. Many studies (e.g., Burstein et al. 1984; Covino et al. 1995; Cohen et al. 1998; Trager et al. 1998; Puzia et al. 2002, hereafter PSK02; Schiavon et al. 2005, hereafter SRC05; Schiavon et al. 2012, hereafter S12; Pipino & Danziger 2011; Roediger et al. 2014) have investigated the line-strength indices from integrated spectra of GGCs. Among them, PSK02 presents a set of Lick indices for 12 GGCs including metal-rich bulge GCs. SRC05 provides the largest set of integrated spectra for 41 GGCs (including most of the PSK02 sample), and S12 presents the Lick index measurements for the spectra later on.

The Lick index system (Burstein et al. 1984; Worthey et al. 1994; Worthey & Ottaviani 1997; Trager et al. 1998) is the most widely used spectral index system, which consists 25 line indices in the optical wavelength range ($4000 \text{ \AA} \lesssim \lambda \lesssim 6400 \text{ \AA}$). This system has been renewed and upgraded by several authors (e.g. Schiavon 2007, Franchini et al. 2010, Vazdekis et al. 2010) along with the improvement of modern instruments. In this paper, we present 20 absorption line indices measured in high-resolution integrated spectra of 24 GGCs, 13 of which are newly observed. The line indices are calibrated to the Lick indices both on the Schiavon (2007) redefinition (hereafter S07) and on the line-index system (hereafter LIS; Vazdekis et al. 2010). Our goal is to provide a combined catalog of widely used line-indices for the largest GGC sample.

The paper is organized as follows: Sections 2 and 3 describe the observation and data reduction, respectively. In Section 4, we construct a homogeneous data set of the Lick

indices on the S07 and LIS systems for 53 GGCs by combining our data with the existing catalogs, and derive empirical index-to-metallicity conversion relations for the Lick indices from the combined catalog. We provide the fully reduced, flux-calibrated GC spectra as well. Section 5 summarizes our results.

2. OBSERVATION

Spectroscopic observations of 24 GGCs were conducted with the 2.5-m Isaac Newton Telescope in La Palma, Spain from July 4–7, 2000. The nights were not photometric. Our sample of GGCs spans a wide range of metallicities, $-2.4 \lesssim [\text{Fe}/\text{H}] \lesssim 0.1$, with a mean metallicity of $[\text{Fe}/\text{H}] \simeq -1.3$, on the Carretta & Gratton (1997) scale. The sample also includes both clusters with blue horizontal branches and red horizontal branches. The basic properties of these GGCs are listed in Table 1. We used the Intermediate Dispersion Spectrograph (IDS) with the 235 camera, the EEV10 CCD detector, the R900V grating, and a long-slit with a width of $1''.5$. Because of the severe vignetting of the 235 camera optics¹, the maximum useful slit length is $3.3'$. This configuration provides a spatial resolution of $0.4 \text{ arcsec pixel}^{-1}$, a wavelength range of $4000 - 5400 \text{ \AA}$, a spectral dispersion of $0.63 \text{ \AA pixel}^{-1}$, and a spectral resolution of $\text{FWHM} \sim 2.0 \text{ \AA}$. The FWHM values measured from arc lines are $\sim 1.94 \text{ \AA}$ and do not show any trend with the wavelength. The slit was drifted $\pm 1 r_c$ from the cluster center, where r_c is the cluster core radius, during an exposure time of 900 seconds. In order to check the self-consistency of our data and foreground star contamination, we repeated exposures with the slit positioned in an orthogonal direction.

For large GCs, separate sky exposures ($15'$ north for NGC 5904 and NGC 6205, and $15'$ north and $15'$ east for NGC 6838) were obtained for background subtraction. The

¹See <http://www.ing.iac.es/astronomy/instruments/ids/ids-eev10.html>

observation date, the number of exposures in each direction, the number of sky exposures, and the extraction windows are listed in Table 2. Figure 1 demonstrates the scan coverage for each GGC on Digitalized Sky Survey images. A total of 47 Lick standard stars were observed for accurate calibration to the standard Lick system. A spectrophotometric standard star was also observed each night for flux calibration. The exposure times for the standards varied from 4 seconds to 10 seconds depending on brightness. Between each repositioning of the telescope, an arc frame was taken using a CuAr/CuHe lamp for wavelength calibration. Each exposure produced a raw image with 500 pixels along the spatial axis and 4200 pixels along the dispersion axis. The CCD gain was $1.17 e^-/\text{ADU}$, and the readout noise was $4.2 e^-/\text{pixel}$.

3. DATA REDUCTION

The raw images were reduced using the standard IRAF package. The basic CCD reduction was performed according to the procedure described in *A User's Guide to CCD Reductions with IRAF* (Massey 1997). The *IRAF/ccdred* package was first used to trim an overscan region and to subtract a bias frame. A flat-field frame and a twilight sky frame for each night were constructed by averaging several separate frames. Then, a normalized flat-field was obtained along the dispersion axis by fitting a fifth-order polynomial function using the *RESPONSE* task in the *twodspec.longslit* package, and a smoothed twilight sky flat was made along the spatial axis using the *ILLUM* task in the same package. By multiplying the previous two products, the ‘ideal’ flat was produced and used for flat fielding of all scientific data as well as the calibration data. Cosmic rays were removed using the *APALL* routine in the IRAF package, which rejects any highly deviated values while optimally extracting a spectrum.

After the basic CCD reduction, spectra were extracted and calibrated following the

procedures in *A User's Guide to Reducing Slit Spectra with IRAF* (Massey, Valdes, & Barnes 1992). The *APALL* routine was used to extract a spectrum from the two-dimensional long-slit spectroscopic images. We set aperture radii for spectra extraction initially as $0.5 r_c$ or $1.0 r_c$ for each GGC, and increased to cover the outer region of the cluster. For NGC 6342, the $0.5 r_c$ extraction window was not used because of the small size of the cluster. For the GGCs that did not have separate sky exposures, sky background regions were defined on both sides well away from the central light profile, avoiding any bright field stars. If one side of the outskirts of a GGC was heavily contaminated by field stars, the other side was selected to estimate the sky background. Figure 2 shows the flux summation along the dispersion direction, visualizing the spectrum extraction regions of the GGCs and the sky background areas. The extraction regions were selected to cover almost the whole area in the spatial axis avoiding any bright stars for images with separate sky exposures. Once these extraction windows for the GGCs and sky backgrounds were defined, the *APALL* routine automatically determined a center for the GGCs in the spatial axis and traced it along the dispersion axis with a ten pixel step size. The process then combined the spectra within the previously defined extraction windows and subtracted the sky spectrum. During this process, cosmic rays were rejected according to three-sigma clipping. For images with independent sky exposures (see Table 2), the sky backgrounds were subtracted manually at the 1D extracted spectrum level. Most results in this work are derived from spectra with an aperture size of $1 r_c$. For standard star calibration, a fixed aperture radius was set at five pixels with a background region between 10 and 20 pixels on each side of the object.

Using CuAr lines in the arc frames for each target, the scientific and calibration data were calibrated with an r.m.s. $\sim 0.2 \text{ \AA}$ precision. Flux calibration was done with the spectrophotometric standard stars Feige110, BD+33-2642, and BD+26-2606 (Oke 1990; Massey et al. 1988). The instrumental sensitivity function was determined using the standard stars from all nights. We verified that the continua of the GC spectra, when

calibrated with the sensitivity function and corrected for reddening using the $E(B - V)$ values from Harris (1996, 2010 edition), show generally good agreements with those of model spectra of the same ages and metallicities with observed GCs predicted from the Yonsei Evolutionary Populations Synthesis (YEPS) model (Chung et al. 2013).

4. RESULTS AND DISCUSSION

4.1. Integrated Spectra

Figure 3 presents the reduced integrated spectra of the GGCs observed in this study. The wavelength- and flux-calibrated GGC spectra are corrected for Galactic extinction and shifted to the rest-frame. We combine all the spectra of each GGC and shifted each spectrum vertically by an arbitrary amount for clarity. The spectra are ordered by increasing metallicity. The GC name with metallicity, horizontal-branch ratio, and signal-to-noise ratio around 4700 Å are denoted above each spectrum. The signal-to-noise ratio per pixel are calculated using the IDL function *DER_SNR* (Stoehr et al. 2008). NGC 6760 is excluded from the figure and further analysis due to its low signal-to-noise ratio.

Comparing the spectra from the two orthogonal slit directions allows to check the self-consistency of our data and any possible field star contamination. Both the drift coverage and the extraction windows are $\pm 1 r_c$ from the center, so that the spectra from the two scan directions cover the same region of the cluster. Hence the two spectra should be identical in principle, despite the different scan directions. This overlapping area is defined by the two orthogonal exposures as shown in Figure 1. The comparison shows that most GCs show good agreement between the spectra obtained from different scan directions. On the other hand, some GCs show differences in spectral shape even between the spectra of the same scan direction. In Figure 4, we present examples of GC spectra showing variances

in the continuum flux level (upper panel) and/or the spectral slope (lower panel) between individual exposures. NGC 6779, NGC 6218, NGC 6717, NGC 6342, and NGC 6304 show flux differences, and NGC 6093 and NGC 7078 show discernible differences in the spectral slope. These disagreements may be due to the telescope pointing errors and the variations in sky conditions during our observations, and to the differences in the sky spectra for the cases where the sky spectra were taken from the edge of the slit. All of these spectral variations would cause uncertainty in spectral indices, and the uncertainty is reflected in the index error estimation as described in Section 4.2.

We provide the wavelength- and flux-calibrated GGC spectra extracted from a series of apertures listed in Table 2. The data are in the multispec FITS format comprised of four bands. The first band contains variance-weighted, cosmic-ray cleaned, background-subtracted spectrum. The second band contains background-subtracted spectrum without variance-weighting and cosmic-ray cleaning. The third band contains background spectrum obtained from a separate sky exposure or the ends of the long slit as mentioned in Section 3. The fourth band contains the sigma spectrum. The spectra are made available at the YEPS² and the MILES³ websites.

4.2. Index Measurements

4.2.1. Radial Velocities

Radial velocities are measured by the penalized pixel-fitting method (pPXF; Cappellari & Emsellem 2004). The method extracts the line-of-sight velocity distributions (LOSVD) described by the Gauss-Hermite series (Gerhard 1993; van der Marel & Franx

²<http://web.yonsei.ac.kr/cosmic>

³<http://miles.iac.es>

1993) by directly fitting observed spectra to template spectra in pixel space. In order to avoid the template-mismatch problem, we use 350 MILES models (Vazdekis et al. 2010) as velocity templates covering a wide range of ages (0.06–17 Gyr) and metallicities ($-2.3 \leq [m/H] \leq 0.2$). The MILES models have a slightly lower spectral resolution than our data (2.51 Å versus 2.0 Å FWHM) and we smooth our spectra to the MILES resolution. Following the procedure described in Cappellari & Emsellem (2004), we determine the optimized penalty parameter for each GGC spectrum which minimizes the uncertainties in fitting with the high order Gauss-Hermite moments (h3 and h4) by biasing the fitting solution towards a Gaussian LOSVD. We then derive the radial velocities by running pPXF on each scan of the target GGCs in the wavelength range of 4000 Å to 5400 Å. The velocity uncertainties are determined as the standard deviation of the velocities measured from 500 Monte Carlo simulations for each GGC spectrum, in which the velocity measurements are repeated with the template spectra slightly modified by adding noise.

To determine the final velocity of each GGC, we compare the velocities measured from different scan directions for the same object. We found that, in some cases, there are significant velocity differences between scan directions, which seems to be originated from the zero point shift in wavelength calibrations. We have taken the arc frames between the repositioning of the telescope but not between the change of the slit direction. This leads to wavelength zero point shift for some objects resulting in the velocity zero-point offsets between the data. We therefore apply zero point corrections to the velocity measurement using the [O I] $\lambda 5577$ night sky line. The final velocity of each GGC is determined as the error-weighted mean of the velocities measured from different scans and the velocity error is computed using standard error propagation procedures.

We note that the typical velocity dispersion of GGCs (< 10 km/s; Dubath et al. 1997) is smaller than our instrumental velocity resolution ($\sigma \sim 54.2$ km s⁻¹). The pPXF method

have had an issue that the kinematics could not be reliably recovered when the velocity dispersion of the object is smaller than the instrumental dispersion. However, the pPXF code has recently been updated solving the issue by adopting the analytic Fourier transform of the LOSVD (for details, see Section 4 of Cappellari 2016). To check the robustness of our measurements, we also measure the radial velocities by Fourier cross-correlation using the *FXCOR* task in IRAF. The measurements are generally in good agreement with each other, whereas the velocity measurement via pPXF method gives more consistent values for the same GGC.

Table 3 lists the final radial velocities and their uncertainties along with the radial velocities from Harris (1996, 2010 edition). Figure 5 compares our measurements and Harris’s values. Our velocities are in generally good agreement with the literature values.

4.2.2. *Measuring the Lick Indices on the S07 System*

S07 proposed a new Lick index system (referred to as S07 system in this paper) which is based on the Jones (1999) spectral library containing a large set of high-resolution, flux-calibrated stellar spectra. By adopting the flux-calibrated standard spectra, the S07 system is free from the possible uncertainties associated with the response curve of the original Lick/IDS spectrograph and achieves a higher accuracy of the Lick indices as illustrated in Figures 1 and 2 of S07.

We measure the equivalent widths (EWs) of the indices for all individual GGC spectra, following the definition of the index passbands provided by Worthey et al. (1994) and Worthey & Ottaviani (1997), which consists 25 line indices in the optical wavelength range ($4000 \text{ \AA} \lesssim \lambda \lesssim 6500 \text{ \AA}$). Our measurements are restricted to 20 indices excluding the five longest wavelength ones (Fe5709, Fe5782, NaD, TiO₁, and TiO₂) because of the

limited wavelength coverage ($4000 \text{ \AA} \lesssim \lambda \lesssim 5400 \text{ \AA}$) of our spectra. Before measuring the indices, we shift our GGC spectra to the rest-frame using the radial velocities determined in Section 4.2.1, and degrade the spectra to the wavelength-dependent resolution of the Lick index system⁴. We then measure the EWs of the indices and index errors from the spectra with the *LICK_EW* code in the *EZ_Ages* IDL package (Graves & Schiavon 2008). The line broadening caused by velocity dispersion is not considered since GCs, unlike galaxies, have very low velocity dispersion ($< 10 \text{ km/s}$; Dubath et al. 1997).

We calibrate the instrumental index measurements to the S07 system using the Lick standard stars. The index measurements for the standard stars are performed in the same way as for the GGCs. In Figure 6, our index measurements for the standard stars are compared with those reported in S07⁵. The differences between the two measurements are generally small compared to the observational error and only minor zero-point offset corrections are needed. The zero-point offsets are determined by calculating the error-weighted mean of the differences after removing outliers by applying a three-sigma clipping procedure. The resulting offsets, $\Delta_{index} = EW_{S07} - EW_{this\ work}$, are listed in Table 4. The instrumental indices are converted to the Lick/S07 system by adding the offset values. The final Lick/S07 indices for each GGC are calculated by the error-weighted mean of the Lick/S07-calibrated indices from multiple exposures, and the index errors are

⁴The resolutions are given in the Table 1 of S07. The S07 system is defined on the original Lick/IDS variable resolution because the index measurements of Worthey et al. (1994) were used as a supplement to the database.

⁵Some indices are not provided by S07 due to gaps in the coverage of the Jones (1999) spectra. For those measurements, we use the Indo-US stellar spectra that are in common with the original Lick/IDS library. We obtained the data via private communication with Schiavon.

determined as the standard deviation of the error-weighted mean.

4.2.3. *Measuring the Lick Indices on the LIS System*

Vazdekis et al. (2010) proposed the LIS system as an alternative to the Lick/IDS system aiming to minimize the uncertainties caused by degrading the observed spectral resolution to the variable resolution of the Lick/IDS definition (8–11 Å). The LIS system is defined on a flux-calibrated spectrum whose spectral resolution is constant along the whole spectral range. The system uses three standard resolutions of 5, 8.4, and 14 Å FWHM, which are suitable for studies of GCs, intermediate-mass galaxies, and massive galaxies, respectively. In this study, we use the same index definition of the Lick system on the 5.0 Å LIS system.

To measure the Lick indices on the LIS system from our data, we smooth our GC spectra with a gaussian using the *GAUSS* task in IRAF with a sigma of 2.9 pixels to give FWHM \sim 5.0 Å. We then shift the spectra to the rest-frame and measure the indices with *LECTOR*⁶ software. The final index values are determined by taking the error-weighted mean of the indices and the uncertainties are estimated by calculating the standard deviation of the error-weighted mean.

Figure 7 shows a comparison between the index measurements for the standard stars in our data and for the stars provided in the MILES stellar library (Vazdekis et al. 2010). The indices on the LIS system, in principle, do not require any calibrations on a standard system if the measurements are based on well flux-calibrated spectra. However, as shown in the figure, there are some offsets which is likely due to the imperfectness of flux-calibrations. Hence, we decide to calibrate our measurements on the LIS system of Vazdekis et al. (2010)

⁶http://www.iac.es/galeria/vazdekis/vazdekis_software.html

by adding the offsets to our measurements. The offsets are given in Table 5.

4.3. Data Compilation and the Combined Catalogs

4.3.1. The Catalog of Lick/S07 Indices

We combine our results with previous catalogs of GGC Lick indices provided by PSK02 and by S12. PSK02 observed 12 GGCs mainly associated with the Galactic bulge using the ESO 1.52-m telescope in La Silla and measured all 25 Lick indices. SRC05 obtained integrated spectra of 41 GGCs with the Cerro Tololo Inter-American Observatory (CTIO) Blanco 4-m telescope and released their calibrated spectra with FWHM ~ 3.1 Å. S12 provides 23 Lick indices—except Fe4531 and Fe5015 due to the CCD defects in their spectral regions (Schiavon et al. 2005; Mendel et al. 2007)—measured from the SRC05 spectra, which are calibrated to the S07 system. There are five common GCs between our data and PSK02, 11 common GCs between our data and S12, and four common GCs in all three sources.

In Figure 8, we compare our index measurements with those of PSK02 and S12 for the common GCs. The systematic difference between our data and PSK02 data arises from the use of different Lick systems: PSK02 use the original Lick/IDS system with the index definition of Worthey & Ottaviani (1997) and Trager et al. (1998) while our data are calibrated to the Lick/S07 system with the index definition of Worthey et al. (1994) and Worthey & Ottaviani (1997). We determine the index offsets, $\Delta_{PSK02} = EW_{this\ work} - EW_{PSK02}$, by computing error-weighted mean values of the differences between the two indices, and convert the PSK02 indices to the Lick/S07 system. The offset values are given in Table 6. On the other hand, the difference between ours and S12 data can be explained by random errors and/or the difference of the observed regions

for a given GC.

The three datasets of Lick/S07 indices are merged to form a new one. For the common GCs, we adopt the error-weighted mean as the final index value. Table 7 provides the combined catalog of 20 Lick/S07 indices for 53 GGCs covering a wide range of metallicities, $-2.4 \lesssim [\text{Fe}/\text{H}] \lesssim 0.1$. The index uncertainties listed under the Lick indices are the standard deviation of the error-weighted mean.

4.3.2. *The Catalog of LIS Indices*

In addition to our spectral data, we use the integrated spectra of 41 GCs provided by SRC05 for constructing a final catalog of the LIS indices. We smooth the SRC05’s spectra with $\text{FWHM} \sim 3.1 \text{ \AA}$ using a gaussian of 1.67 pixel sigma to match the LIS-5.0 \AA resolution. We then measure the LIS indices with *LECTOR* software from the spectra. For the multiple exposures of the same GC, the final index values are determined by taking the error-weighted mean of the index measurements and the uncertainties are estimated by calculating the standard deviation of the error-weighted mean.

The two datasets are combined to create the final LIS index catalog of a total of 53 GGCs. For the 11 common GCs in the two datasets, there are small zero point offsets which are likely due to the differences in the flux calibration between the two datasets as mentioned in Section 4.2.3. Before combining the two datasets, the zero point offset corrections are applied. For the Fe4531 and Fe5015 indices, we do not use the measurements of SRC05 data because of the known problems in their spectra. The index values adopted for the common GCs are the error-weighted mean of the two measurements and the uncertainties are determined by the standard deviation of the error-weighted mean. The final LIS index catalog is given in Table 8.

4.4. The Empirical Index–Metallicity Relations

This Section provides empirical index–metallicity relations (IMRs) based on our combined index catalogs of 53 GGCs. One can use the IMRs to estimate the metallicities of extragalactic GCs. Determining the metallicities of extragalactic GCs is, however, not a straightforward task because of the well-known age–metallicity degeneracy, the effect of α -elements enhancement, and even the ambiguity of the term “metallicity” (e.g., Puzia et al. 2002; Beasley et al. 2008). On the one hand, the metallicities of GGCs are relatively well constrained because they can be estimated from various ways including direct observations for the cluster member stars (e.g., Malavolta et al. 2014, Valenti et al. 2015, Mészáros et al. 2015). Hence, with an assumption that extragalactic GCs are analogous to GGCs, calibrating the metallicity of extragalactic GCs to that of GGCs using the IMRs is a useful way to study the nature of extragalactic GCs (e.g., Brodie & Huchra 1990; Cohen et al. 1998; Kissler-Patig et al. 1998; Nantais et al. 2010; Pipino & Danziger 2011; Park et al. 2012). The IMRs are also useful for validating and calibrating theoretical stellar population models, as they provide observational constraints for comparison with model predictions (e.g., Chung et al. 2013; Kim et al. 2013).

We derive the empirical relations between both the Lick/S07 and the LIS indices and metallicity using our combined GGC catalog. The metallicity values are taken from Carretta et al. (2009) who updated the scale of Carretta & Gratton (1997) metallicity scale. Because both variables—spectral index and metallicity—have measurement errors, we adopt an orthogonal distance regression method (Boggs & Rogers 1990) to determine the best-fit polynomial function. During the fitting procedure, outliers are rejected by applying the three-sigma clipping method.

Figure 9 shows the IMRs for 20 Lick/S07 indices. The blue, green, and red solid lines

represent first-, second-, and third-order polynomial functions, respectively, i.e.,

$$[\text{Fe}/\text{H}] = a_0 + a_1 \times (\text{index}), \quad (1)$$

$$[\text{Fe}/\text{H}] = a_0 + a_1 \times (\text{index}) + a_2 \times (\text{index})^2, \text{ and} \quad (2)$$

$$[\text{Fe}/\text{H}] = a_0 + a_1 \times (\text{index}) + a_2 \times (\text{index})^2 + a_3 \times (\text{index})^3. \quad (3)$$

The units of *index* are mag for CN₁, CN₂, Mg₁, and Mg₂ and angstrom for the other indices. We also present the 95% confidence bands of the LOESS regression, a nonparametric locally weighted regression (Cleveland 1994), as gray-shaded regions for a visual comparison of the polynomial fits with the underlying trend of the data. The polynomial coefficients are given in Table 9 (for the first order fit), Table 10 (second order), and Table 11 (third order). We also provide the Bayesian information criterion (BIC; Schwarz, G. 1978), which is a statistical criterion for model selection where the model with the lowest BIC would be the best model. The BIC comparison between the polynomial fits show that the higher-order polynomials (green and red solid lines) give better fits than the first-order polynomial (blue solid line) for most indices, which indicates the nonlinearity of the IMRs. The nonlinearity is also implied by the LOESS results, particularly at the high and low metallicity ends. The IMRs should be valid only in the range from the minimum to maximum values of each index, which are listed in the last columns of Tables 9–11.

Figure 10 shows the IMRs for 20 LIS indices in the same format as in Figure 9. Similar to Lick/S07 IMRs, the higher-order polynomials give better fit in general. The polynomial coefficients are given in Table 12 (first order), Table 13 (second order), and Table 14 (third order) along with the BIC. The valid ranges of relations are given in the last columns of Tables 12–14.

A recent study by Caldwell et al. (2011) and Kim et al. (2013) showed with high precision spectroscopy of 280 GCs in M31 that strong inflection exists in the relations

between metallicity and Balmer lines ($H\beta$, $H\gamma_F$, and $H\delta_F$) and appreciable nonlinearity between metallicity and the Mgb line. Such nonlinear IMRs have been predicted by several stellar population simulation models which incorporate core helium burning horizontal-branch stars in GCs (e.g., Lee & Worthey 2005; Yoon et al. 2006; Chung et al. 2013). In our catalog data, although not conclusive, the relationships between metallicity and Balmer lines appear inflected. For Mgb , the nonlinear feature is weaker in our GGC data than that seen in the M31 GC data (Kim et al. 2013). This is probably due to the smaller sample size and the larger observational errors of our data compared to Caldwell et al. (2011) and Kim et al. (2013) and/or to the larger intrinsic scatter in parameters such as age and α -element mixture. A detailed discussion on the nonlinearity issue is beyond the scope of this paper, and we refer the interested reader to Yoon et al. (2006, 2011a,b, 2013) for further discussion.

5. SUMMARY

- We obtained integrated spectra of 24 Galactic globular clusters with a high spectral resolution of $\text{FWHM} \sim 2 \text{ \AA}$ using the 2.5-m Isaac Newton Telescope in La Palma, Spain. Our cluster sample spans a wide range of metallicities, $-2.4 \lesssim [\text{Fe}/\text{H}] \lesssim 0.1$, and various horizontal-branch morphologies.
- We measured 20 Lick indices in the wavelength range of $4000 \text{ \AA} \lesssim \lambda \lesssim 5400 \text{ \AA}$ from the spectra. The Lick indices are calibrated both on the S07 and LIS systems, which are newly defined Lick index systems based on the modern stellar libraries. We also measured the LIS indices from the spectra of 41 Galactic globular clusters provided by Schiavon et al. (2005) in the same manner.
- For the largest Galactic globular cluster sample (53 clusters), we constructed combined catalogs of 20 Lick indices on the S07 and LIS systems using our data and the data

sets provided by Puzia et al. (2002) and Schiavon et al. (2005).

- The combined catalogs and the fully reduced, flux-calibrated spectra can be found in the YEPS and MILES websites.
- We derived the empirical index-to-metallicity conversion relations for both the Lick/S07 and the LIS indices, which can be used for extragalactic globular cluster studies.

S.-J.Y. acknowledges support by Mid-career Research Program (No. 2015-008049) through the National Research Foundation (NRF) of Korea, the NRF of Korea to the Center for Galaxy Evolution Research (No. 2010-0027910), and the Yonsei University Future-leading Research Initiative of 2015-2016. This work was supported in part by the Yonsei University Research Fund of 2013. M.B. and A.V. acknowledge support from the Programa Nacional de Astronomía y Astrofísica of MINECO, under grant AYA2013-48226-C3-1-P.

REFERENCES

- Beasley, M. A., Bridges, T., Peng, E., et al. 2008, *MNRAS*, 386, 1443
- Boggs, P. T. & Rogers, J. E. 1990, Orthogonal Distance Regression, in *Statistical analysis of measurement error models and applications: proceedings of the AMS-IMS-SIAM joint summer research conference held June 10-16, 1989*, *Contemporary Mathematics*, 112, 186
- Brodie, J. P., & Huchra, J. P. 1990, *ApJ*, 362, 503
- Burstein, D., Faber, S. M., Gaskell, C. M., & Krumm, N. 1984, *ApJ*, 287, 586
- Caldwell, N., Schiavon, R., Morrison, H., Rose, J. A., & Harding, P. 2011, *AJ*, 141, 61
- Cappellari, M. 2016, arXiv:1607.08538
- Cappellari, M., & Emsellem, E. 2004, *PASP*, 116, 138
- Carretta, E., Bragaglia, A., Gratton, R., D’Orazi, V., & Lucatello, S. 2009, *A&A*, 508, 695
- Carretta, E., & Gratton, R. G. 1997, *A&AS*, 121, 95
- Chung, C., Yoon, S.-J., Lee, S.-Y., & Lee, Y.-W. 2013, *ApJS*, 204, 3
- Cleveland, W. S. 1994, *The Elements of Graphing Data* (2nd ed.; Summit: Hobart Press)
- Cohen, J. G., Blakeslee, J. P., & Ryzhov, A. 1998, *ApJ*, 496, 808
- Covino, S., Galletti, S., & Pasinetti, L. E. 1995, *A&A*, 303, 79
- Dubath, P., Meylan, G., & Mayor, M. 1997, *A&A*, 324, 505
- Franchini, M., Morossi, C., Di Marcantonio, P., Malagnini, M. L., & Chavez, M. 2010, *ApJ*, 719, 240

Gerhard, O. E. 1993, MNRAS, 265, 213

Graves, G. J., & Schiavon, R. P. 2008, ApJS, 177, 446

Harris, W.E. 1996, AJ, 112, 1487

Jones, C. D. 1999, Ph.D. Thesis, 4003

Kim, S., Yoon, S.-J., Chung, C., et al. 2013, ApJ, 768, 138

Kissler-Patig, M., Brodie, J. P., Schroder, L. L., et al. 1998, AJ, 115, 105

Lee, Y.-W., Demarque, P., & Zinn, R. 1994, ApJ, 423, 248

Lee, H.-c., & Worthey, G. 2005, ApJS, 160, 176

Malavolta, L., Sneden, C., Piotto, G., et al. 2014, AJ, 147, 25

Massey, P. 1997, A User's Guide to CCD Reductions with IRAF

Massey, P., Strobel, K., Barnes, J. V., & Anderson, E. 1988, ApJ, 328, 315

Massey, P., Valdes, F., & Barnes, J. 1992, A User's Guide to CCD Reductions with IRAF

Mendel, J. T., Proctor, R. N., & Forbes, D. A. 2007, MNRAS, 379, 1618

Mészáros, S., Martell, S. L., Shetrone, M., et al. 2015, AJ, 149, 153

Nantais, J. B., Huchra, J. P., Barmby, P., & Olsen, K. A. G. 2010, AJ, 139, 1178

Oke, J. B. 1990, AJ, 99, 1621

Park, H. S., Lee, M. G., Hwang, H. S., et al. 2012, ApJ, 759, 116

Pipino, A., & Danziger, I. J. 2011, A&A, 530, A22

Puzia, T. H., Saglia, R. P., Kissler-Patig, M., et al. 2002, A&A, 395, 45

- Roediger, J. C., Courteau, S., Graves, G., & Schiavon, R. P. 2014, *ApJS*, 210, 10
- Schiavon, R. P., Rose, J. A., Courteau, S., & MacArthur, L. A. 2005, *ApJS*, 160, 163
- Schiavon, R. P. 2007, *ApJS*, 171, 146
- Schiavon, R. P., Caldwell, N., Morrison, H., et al. 2012, *AJ*, 143, 14
- Schwarz, G. 1978, *Annals of Statistics*, 6, 461
- Stoehr, F., White, R., Smith, M., et al. 2008, *Astronomical Data Analysis Software and Systems XVII*, 394, 505
- Trager, S. C., Worthey, G., Faber, S. M., et al. 1998, *ApJS*, 116, 1
- Worthey, G., Faber, S. M., Gonzalez, J. J., & Burstein, D. 1994, *ApJS*, 94, 687
- Worthey, G., & Ottaviani, D. L. 1997, *ApJS*, 111, 377
- Yoon, S.-J., Lee, S.-Y., & Blakeslee, J. P. et al. 2011a, *ApJ*, 743, 150
- Yoon, S.-J., Sohn, S. T., & Kim, H.-S. et al. 2013, *ApJ*, 768, 137
- Yoon, S.-J., Sohn, S.-T., & Lee, S.-Y. et al. 2011b, *ApJ*, 743, 149
- Yoon, S.-J., Yi, S. K., & Lee, Y. 2006, *Science*, 311, 1129
- Valenti, E., Origlia, L., Mucciarelli, A., & Rich, R. M. 2015, *A&A*, 574, A80
- van der Marel, R. P., & Franx, M. 1993, *ApJ*, 407, 525
- Vazdekis, A., Sánchez-Blázquez, P., Falcón-Barroso, J., et al. 2010, *MNRAS*, 404, 1639

Table 1. Sample GC properties

Name	Other Name	l [°]	b [°]	R_{gc} [kpc]	$[\text{Fe}/\text{H}]_{Harr}$	$[\text{Fe}/\text{H}]_{Carr}$	HBR
		(1)	(2)	(3)	(4)	(5)	(6)
NGC 5904	M5	3.86	46.80	6.2	−1.29	−1.33	0.31
NGC 6093	M80	352.67	19.46	3.8	−1.75	−1.75	0.93
NGC 6171	M107	3.37	23.01	3.3	−1.02	−1.03	−0.73
NGC 6205	M13	59.01	40.91	8.4	−1.53	−1.58	0.97
NGC 6218	M12	15.72	26.31	4.5	−1.37	−1.33	0.97
NGC 6229		73.64	40.31	29.8	−1.47	−1.43	0.24
NGC 6304		355.83	5.38	2.3	−0.45	−0.37	−1.00
NGC 6341	M92	68.34	34.86	9.6	−2.31	−2.35	0.91
NGC 6342		4.90	9.72	1.7	−0.55	−0.49	−1.00
NGC 6356		6.72	10.22	7.5	−0.40	−0.35	−1.00
NGC 6517		19.23	6.76	4.2	−1.23	−1.24	...
NGC 6528		1.14	−4.17	0.6	−0.11	0.07	−1.00
NGC 6626	M28	7.80	−5.58	2.7	−1.32	−1.46	0.90
NGC 6638		7.90	−7.15	2.2	−0.95	−0.99	−0.30
NGC 6717	Pal 9	12.88	−10.90	2.4	−1.26	−1.26	0.98
NGC 6760		36.11	−3.92	4.8	−0.40	−0.40	−1.00
NGC 6779	M56	62.66	8.34	9.2	−1.98	−2.00	0.98
NGC 6838	M71	56.75	−4.56	6.7	−0.78	−0.82	−1.00
NGC 6864	M75	20.30	−25.75	14.7	−1.29	−1.29	−0.07
NGC 6934		52.10	−18.89	12.8	−1.47	−1.56	0.25

Table 1—Continued

Name	Other Name	l [°]	b [°]	R_{gc} [kpc]	$[\text{Fe}/\text{H}]_{Harr}$	$[\text{Fe}/\text{H}]_{Carr}$	HBR
		(1)	(2)	(3)	(4)	(5)	(6)
NGC 6981	M72	35.16	−32.68	12.9	−1.42	−1.48	0.14
NGC 7006		63.77	−19.41	38.5	−1.52	−1.46	−0.28
NGC 7078	M15	65.01	−27.31	10.4	−2.37	−2.33	0.67
NGC 7089	M2	53.37	−35.77	10.4	−1.65	−1.66	0.96

Note. — (1) Galactic longitude; (2) Galactic latitude; (3) Distance from Galactic center; (4) Metallicity from Harris (1996, 2010 edition); (5) Metallicity from Carretta et al. (2009); (6) Horizontal-branch ratio defined as $HBR \equiv (B - R)/(B + V + R)$ by Lee et al. (1994), where B and R are the number of stars bluer and redder than the instability strip respectively and V is the number of RR Lyrae stars. The data are taken from Harris (1996, 2010 edition) except $[\text{Fe}/\text{H}]_{Carr}$.

Table 2. Observation log

Night	Object Name	S-N ^a	W-E ^b	Sky ^c	Extraction Windows (r_c)
4 Jul 2000	NGC 5904 (M5)	2	2	2	0.5, 1, 2, 3, 4
	NGC 6171 (M107)	2	2		0.5, 1, 2, 3
	NGC 6229	2	2		0.5, 1, 2, 3, 4, 5
	NGC 6838 (M71)	2	2	4	0.5, 1, 1.5, 2, 2.5
	NGC 7089 (M2)	2	2		0.5, 1, 2, 3, 4
5 Jul 2000	NGC 6205 (M13)	2	2	1	0.5, 1, 1.5, 2
	NGC 6528	2	2		0.5, 1, 2, 3, 4
	NGC 6341 (M92)	2	2		0.5, 1, 2, 3, 4
	NGC 6934	2	2		0.5, 1, 2, 3, 4
	NGC 7006	2	2		0.5, 1, 2, 3, 4
	NGC 7078 (M15)	2	2		0.5, 1, 2, 3, 5, 10
6 Jul 2000	NGC 6517	2	2		0.5, 1, 2, 3, 5, 10
	NGC 6356	2	2		0.5, 1, 2, 3, 4
	NGC 6638	2	2		0.5, 1, 2, 3, 4
	NGC 6717	2	2		0.5, 1, 2, 3, 4
	NGC 6864 (M75)	2	2		0.5, 1, 2, 3, 4
	NGC 6981 (M72)	2	2		0.5, 1, 1.5, 2, 2.5
7 Jul 2000	NGC 6093 (M80)	2	1		0.5, 1, 2, 3, 4, 5
	NGC 6304	2	2		0.5, 1, 2, 3
	NGC 6218 (M12)	3	1		0.5, 1, 1.5, 2

Table 2—Continued

Night	Object Name	S-N ^a	W-E ^b	Sky ^c	Extraction Windows (r_c)
	NGC 6342	0	3		1, 2, 4, 6
	NGC 6626 (M28)	0	2		0.5, 1, 2, 3
	NGC 6779 (M56)	2	2		0.5, 1, 2, 3
	NGC 6760	2	0		0.5, 1, 2, 3

^aNumber of exposures in the South-North scan direction

^bNumber of exposures in the West-East scan direction

^cSeparate sky exposures were taken for three bright extended globular clusters to obtain a better sky subtraction. In other cases, sky spectra were taken from the ends of the long slit.

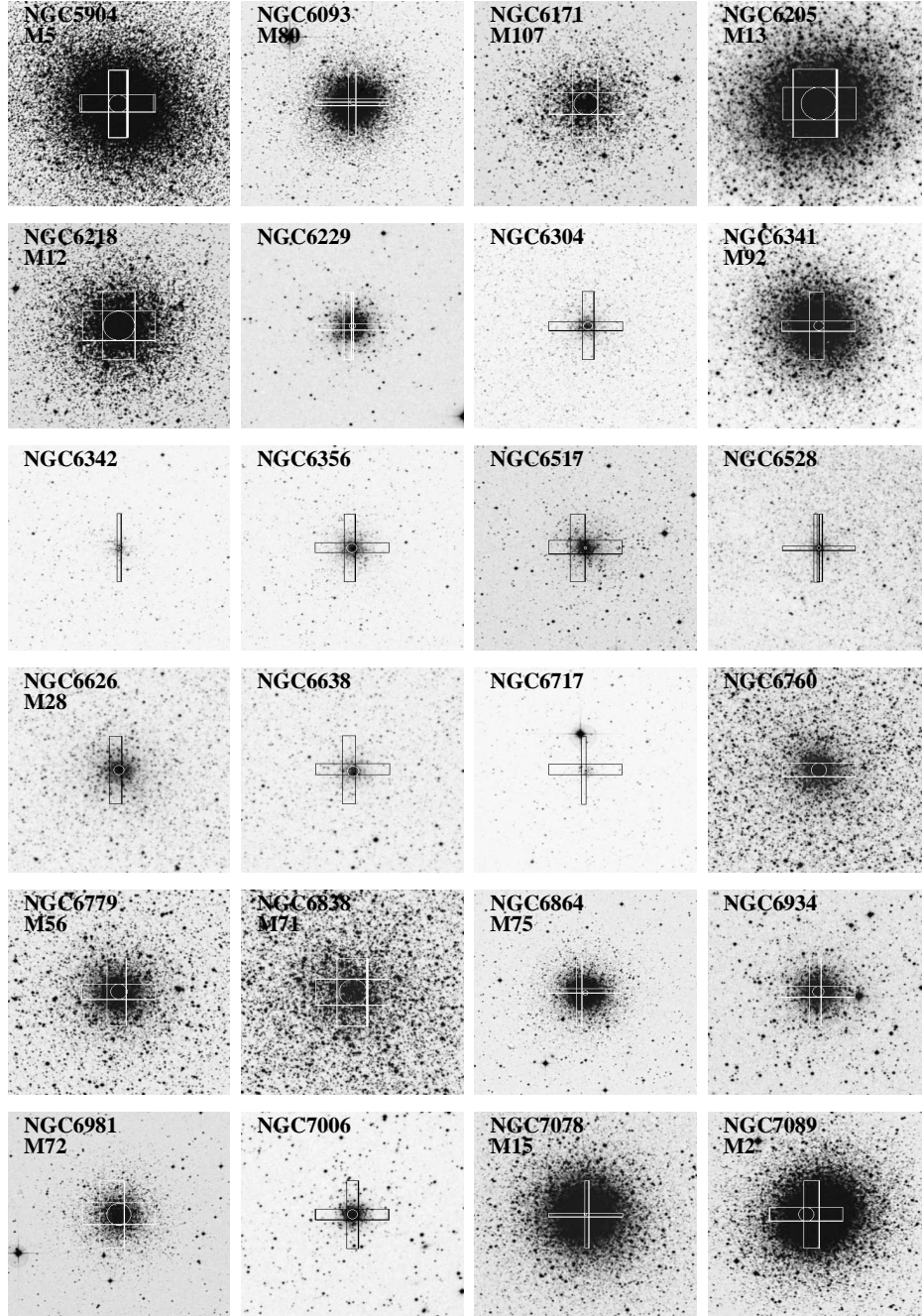


Fig. 1.— Digitalized Sky Survey images of the GGCs observed along with the slit coverages. The circle in the center of each GC represents the core radius. In each rectangle, the long dimension is the slit size, and the short dimension is the drift coverages determined to cover a core radius from the center. The slit position and covering area are drawn based on the telescope positions in image headers from our observations and may have some pointing uncertainties.

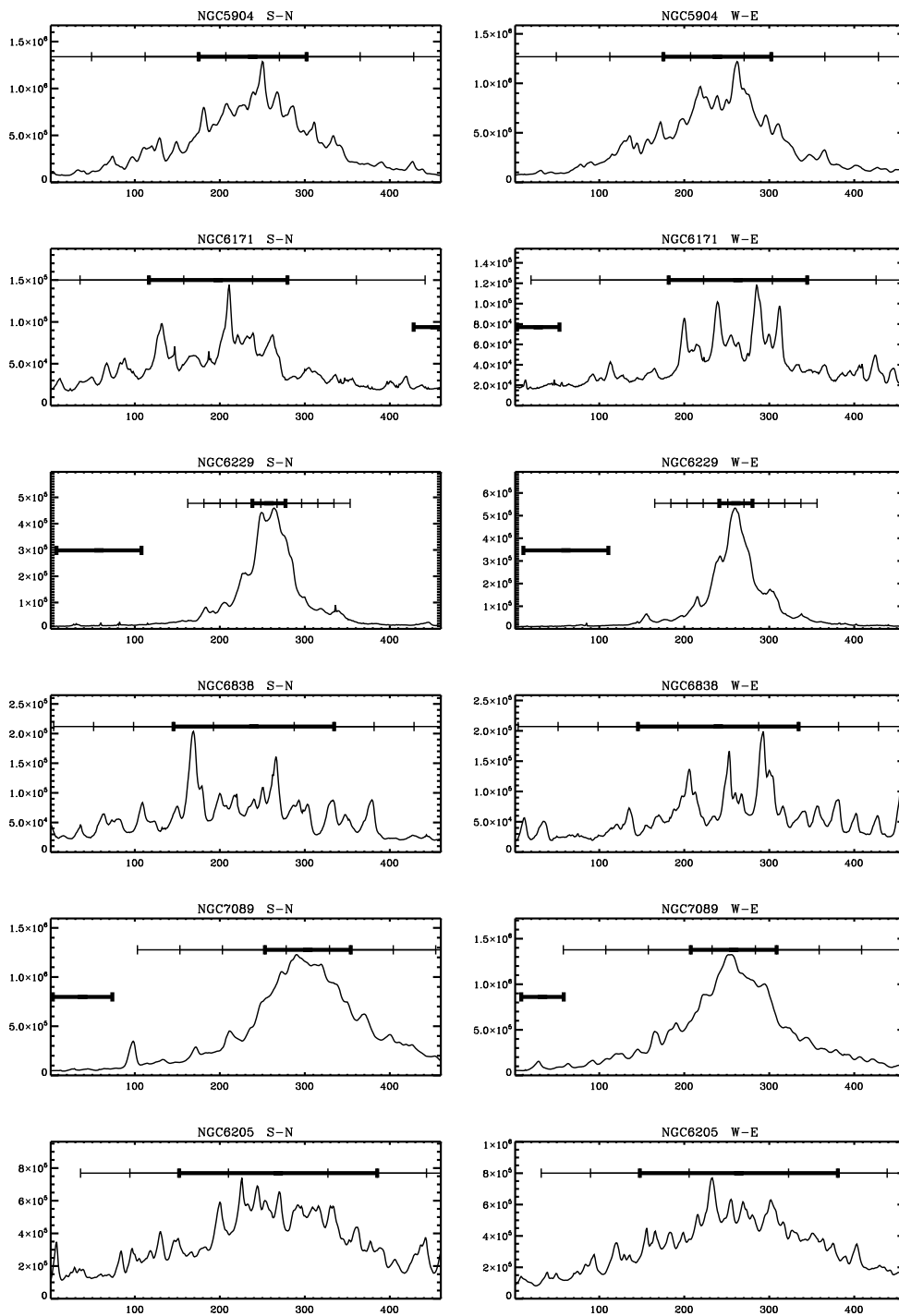


Fig. 2.— Observed light profiles of the 24 GICs. The profiles were obtained by adding flux along the dispersion axis. The x-axis is in pixels and the y-axis is in flux units. In each panel, the upper bars indicate various extraction windows with the thick upper bar equal to the size of the core radius. Lower thick bars represent extraction windows of the background sky selected well away from the globular cluster.

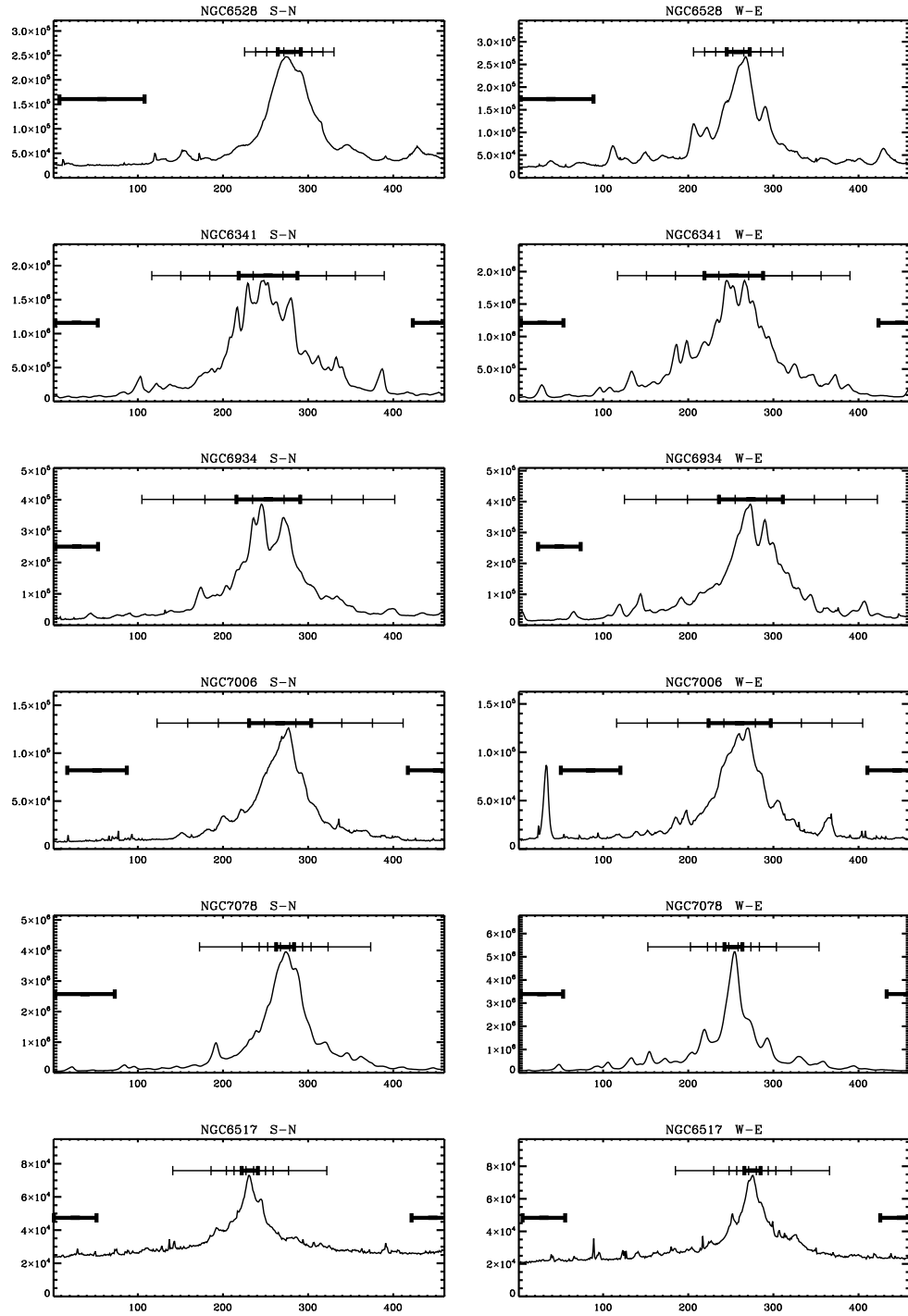


Fig. 2.— Continued.

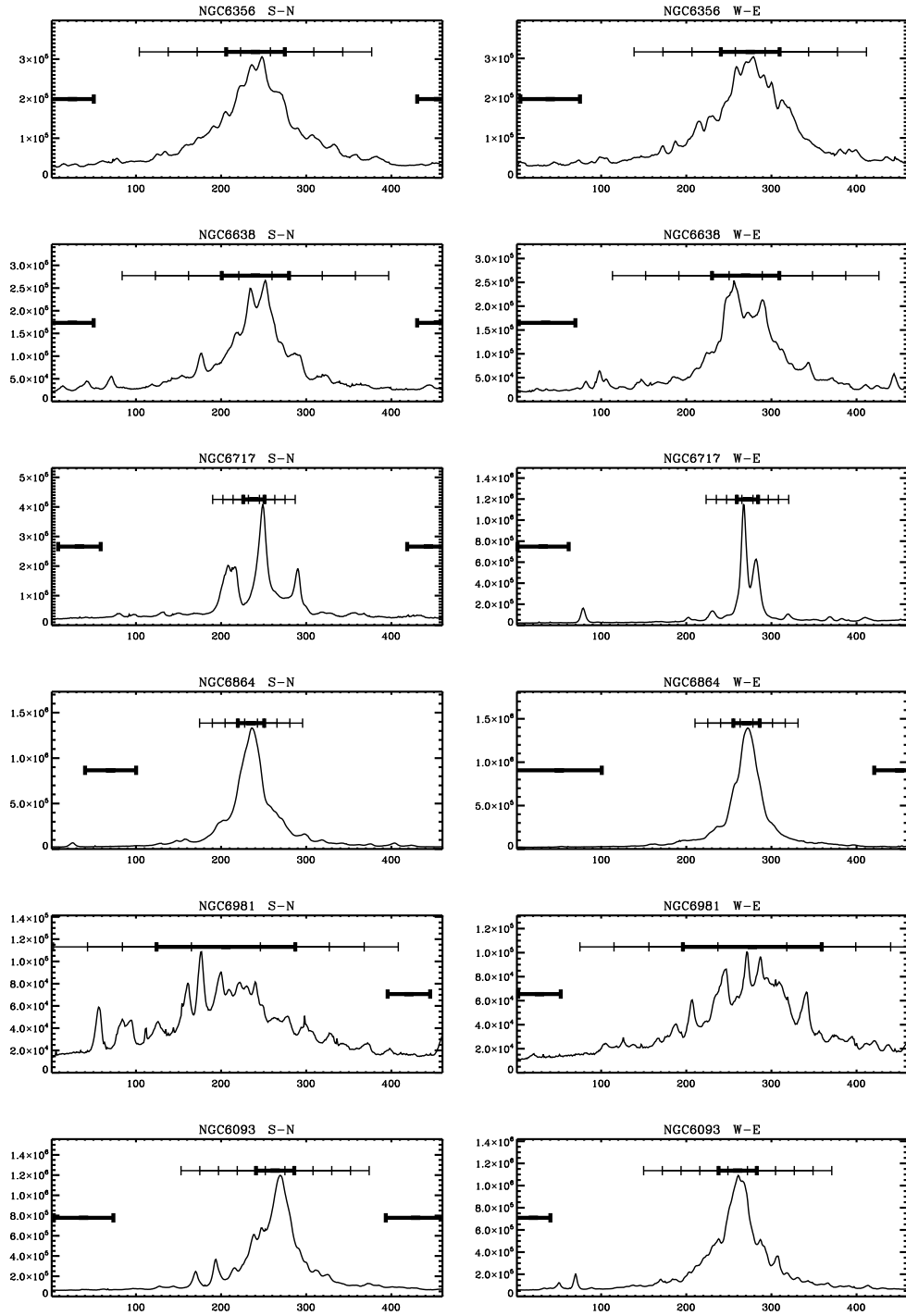


Fig. 2.— Continued.

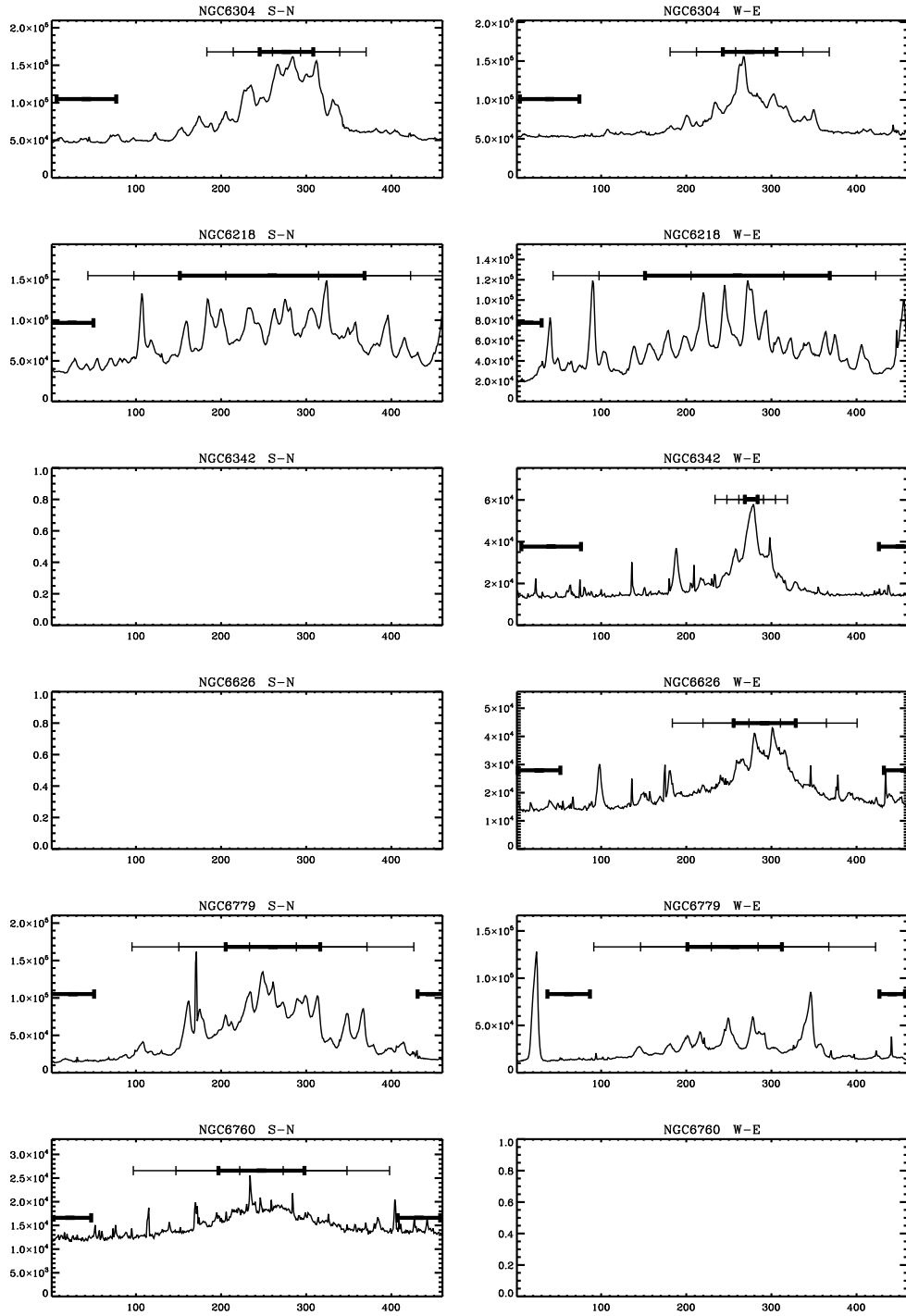


Fig. 2.— Continued.

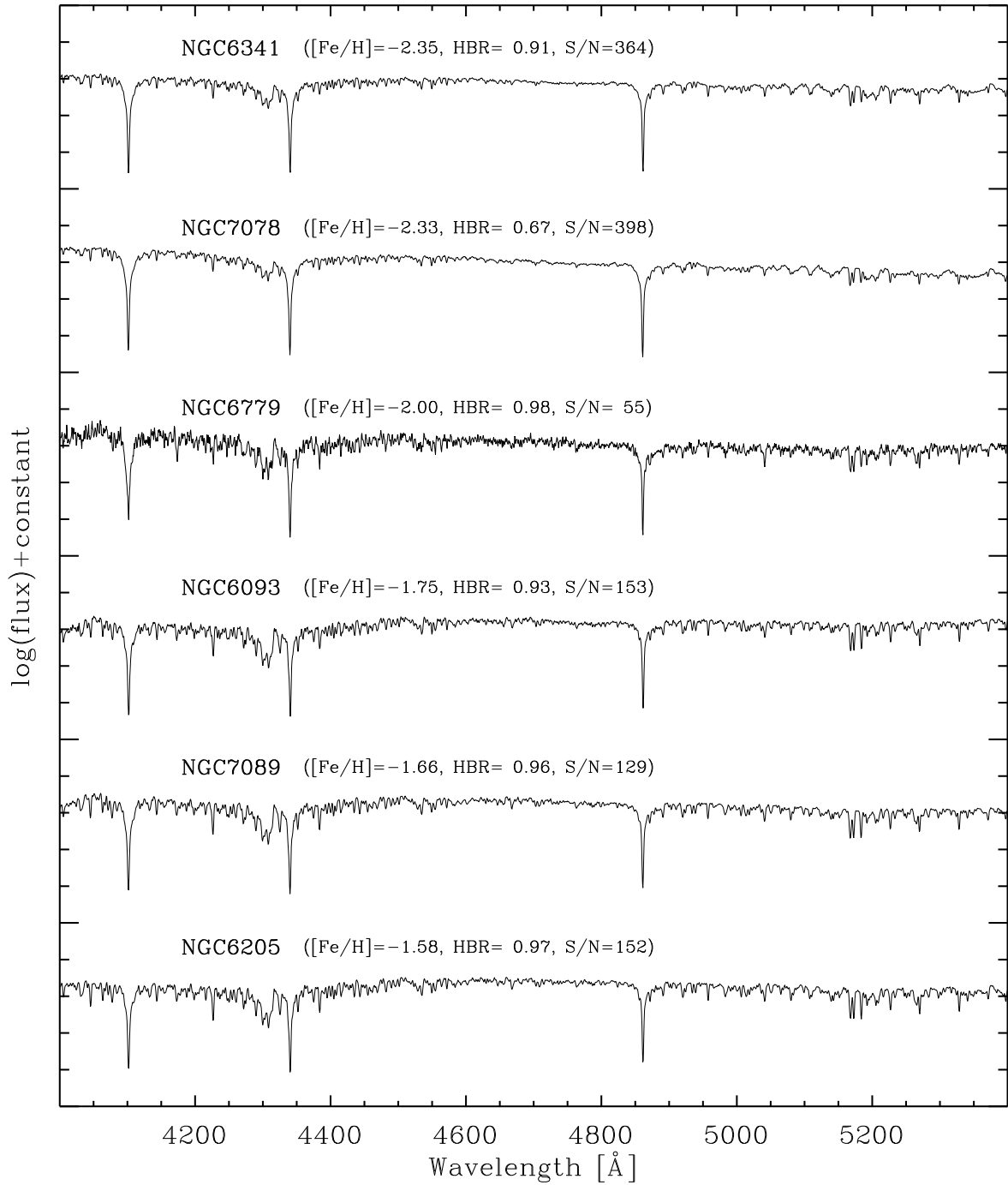


Fig. 3.— Flux-calibrated, dereddened, combined spectra of the observed GGCs. The spectra are ordered by metallicity and shifted vertically by arbitrary constants for clarity. GC names with metallicity, horizontal-branch ratio, and signal-to-noise ratio near 4700 Å are denoted above the respective spectra.

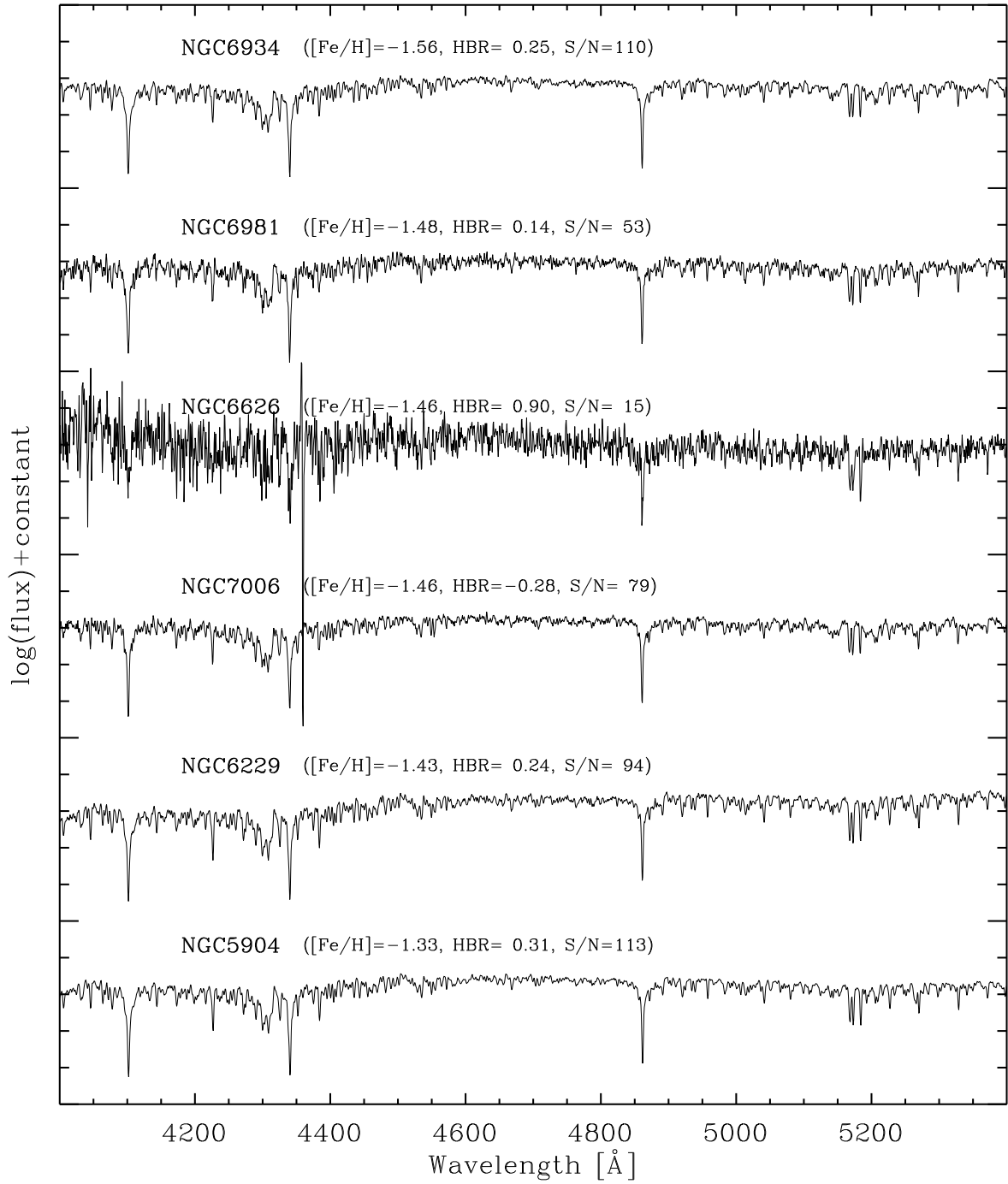


Fig. 3.— continued.

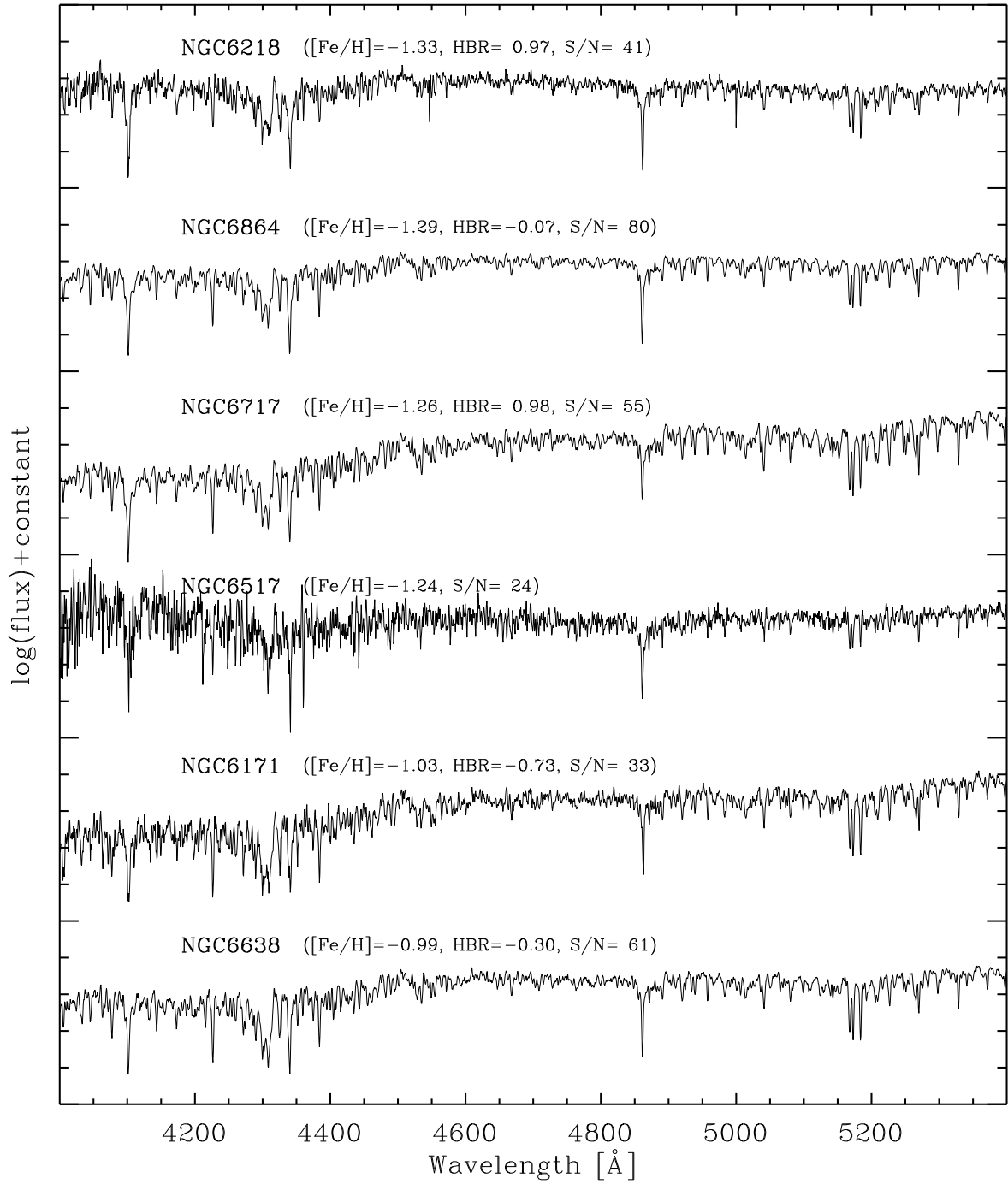


Fig. 3.— continued.

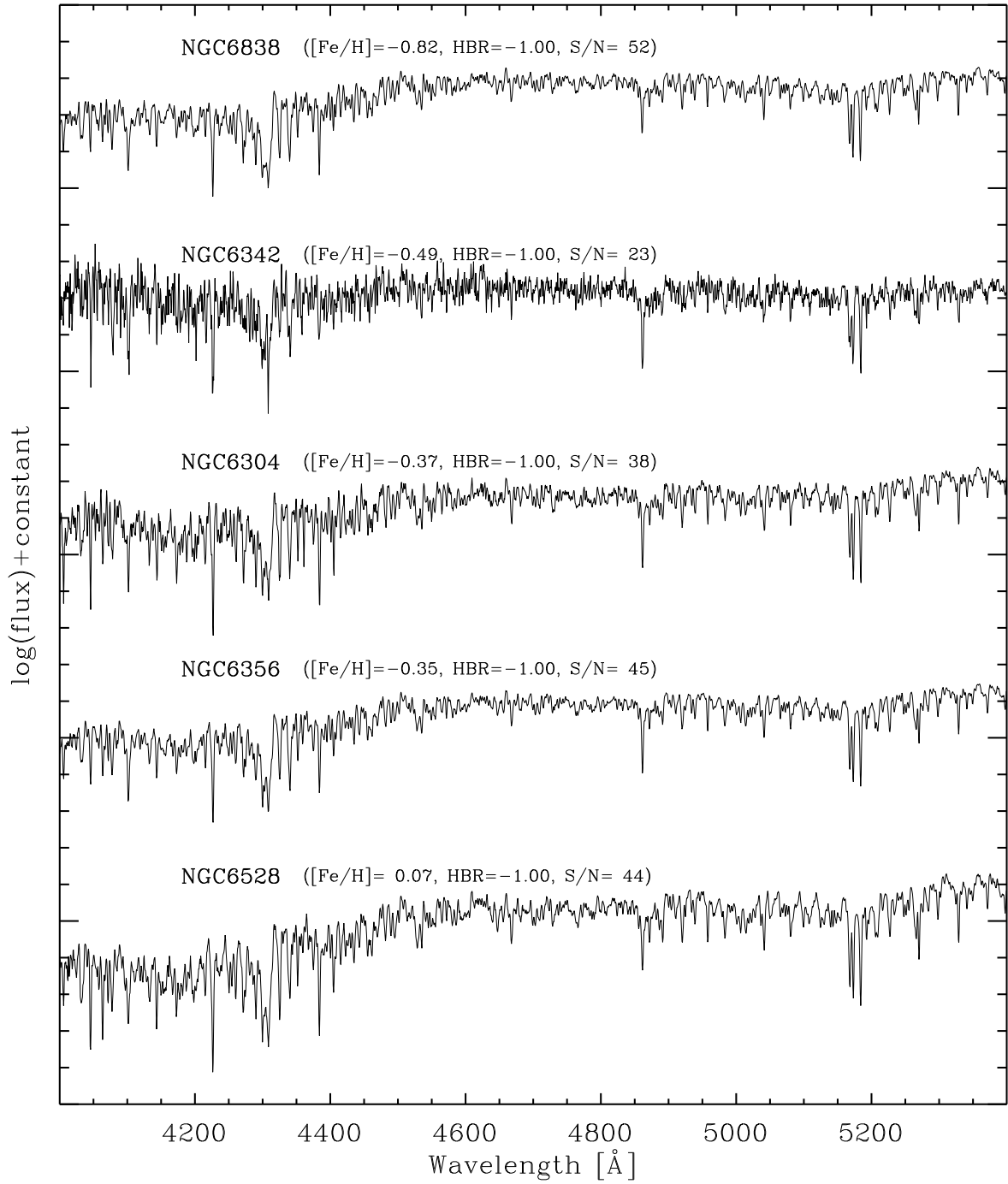


Fig. 3.— continued.

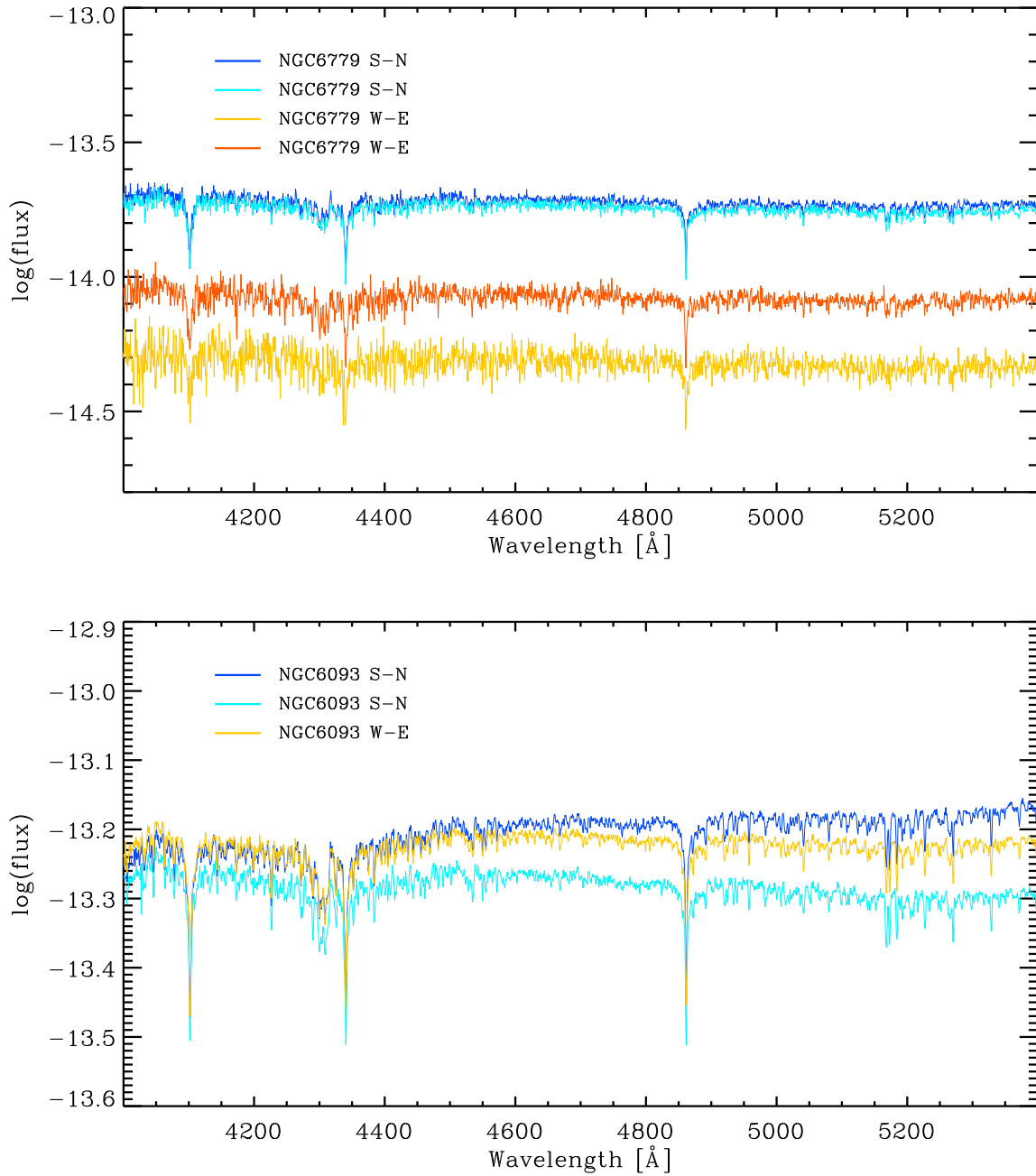


Fig. 4.— Differences in spectral shape between individual spectra for the same GC. The spectra of NGC 6779 (upper panel) show a difference in continuum flux level between exposures, while the spectra of NGC 6093 show a difference in the spectral slope.

Table 3. Radial velocities of sample GCs

GC	$V^a_{r,this\ work}[\text{km/s}]$	$V^b_{r,ref}[\text{km/s}]$
NGC 5904	53.9 ± 3.5	53.2 ± 0.4
NGC 6093	4.2 ± 3.5	8.1 ± 1.5
NGC 6171	-42.6 ± 4.0	-34.1 ± 0.3
NGC 6205	-244.8 ± 3.7	-244.2 ± 0.2
NGC 6218	-56.7 ± 3.1	-41.4 ± 0.2
NGC 6229	-141.5 ± 7.0	-154.2 ± 7.6
NGC 6304	-104.8 ± 3.3	-107.3 ± 3.6
NGC 6341	-105.2 ± 5.8	-120.0 ± 0.1
NGC 6342	128.9 ± 4.2	115.7 ± 1.4
NGC 6356	42.2 ± 3.5	27.0 ± 4.3
NGC 6517	-34.0 ± 4.6	-39.6 ± 8.0
NGC 6528	208.7 ± 5.0	206.6 ± 1.4
NGC 6626	13.8 ± 8.9	17.0 ± 1.0
NGC 6638	11.2 ± 3.5	18.1 ± 3.9
NGC 6717	28.7 ± 3.7	22.8 ± 3.4
NGC 6760	-38.1 ± 9.9	-27.5 ± 6.3
NGC 6779	-138.2 ± 3.4	-135.6 ± 0.9
NGC 6838	-21.4 ± 3.5	-22.8 ± 0.2
NGC 6864	-184.6 ± 3.8	-189.3 ± 3.6
NGC 6934	-406.7 ± 3.9	-411.4 ± 1.6
NGC 6981	-333.5 ± 4.2	-345.0 ± 3.7

Table 3—Continued

GC	$V^a_{r,this\ work}[\text{km/s}]$	$V^b_{r,ref}[\text{km/s}]$
NGC 7006	-383.2 ± 4.3	-384.1 ± 0.4
NGC 7078	-98.4 ± 3.7	-107.0 ± 0.2
NGC 7089	-6.4 ± 3.5	-5.3 ± 2.0

^aThis work

^bTaken from Harris (1996, 2010 edition)

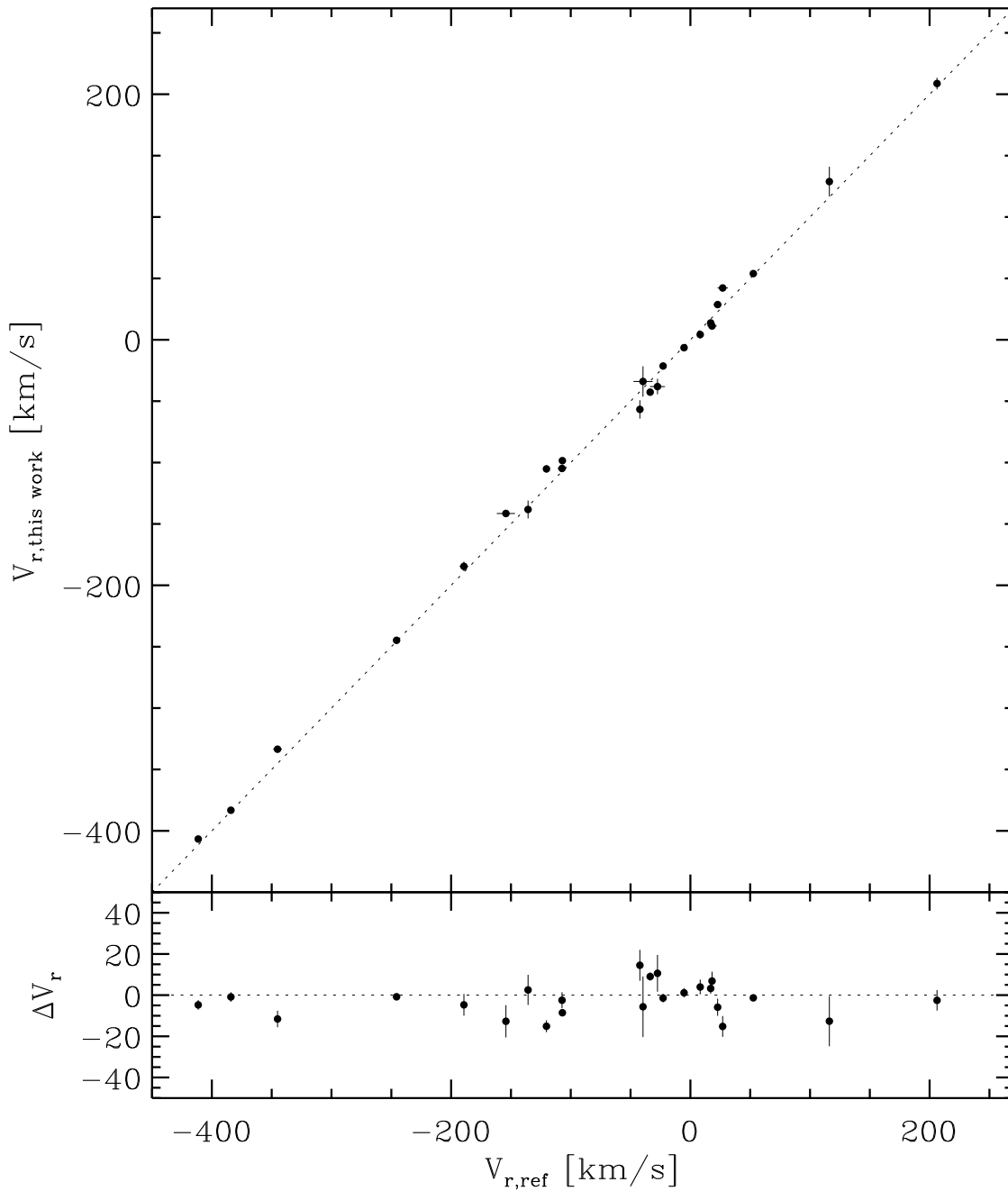


Fig. 5.— Galactic globular cluster radial velocity comparisons. In the upper panel, our measurements are on the y-axis, and the values from Harris (1996, 2010 edition) are on the x-axis. The dotted line represents a one-to-one relationship. The data points are listed in Table 3. In the lower panel, the differences of the two measurements, $\Delta V_r = V_{r,ref} - V_{r,this\ work}$, are plotted.

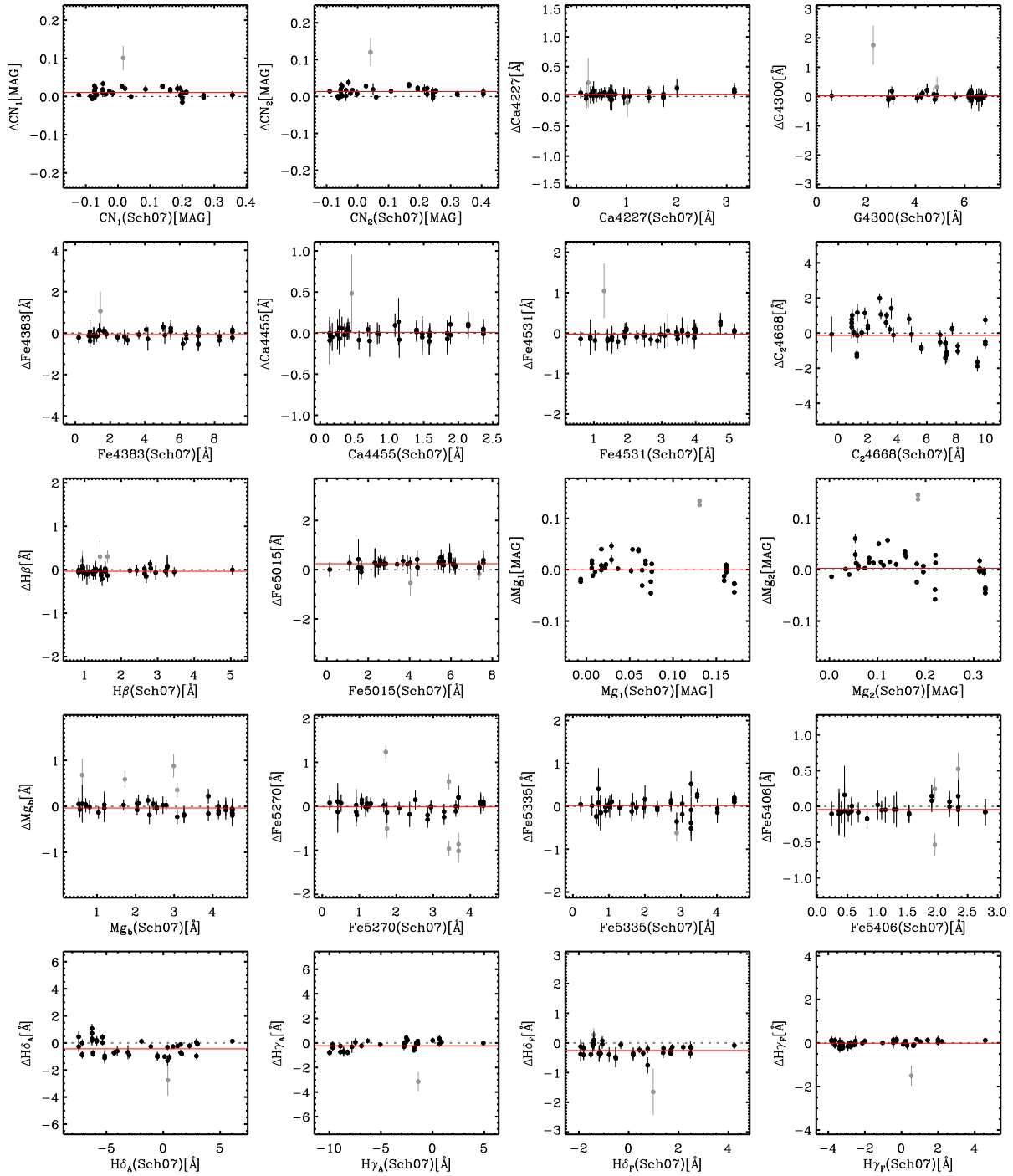


Fig. 6.— Comparison of 20 Lick index measurements for the calibration stars with those reported in S07. The red solid lines represent the offsets between the two datasets, which are determined by calculating the error-weighted mean values of the index measurement differences after removing outliers (gray dots) with three-sigma clipping.

Table 4. Lick index offsets between ours and the S07 data

Line Index	Δ_{Lick}^a
CN ₁	0.0105 ± 0.0009 mag
CN ₂	0.0135 ± 0.0011 mag
Ca4227	0.04 ± 0.02 Å
G4300	0.03 ± 0.03 Å
Fe4383	-0.07 ± 0.04 Å
Ca4455	0.01 ± 0.02 Å
Fe4531	-0.02 ± 0.03 Å
C ₂ 4668	-0.13 ± 0.05 Å
H β	-0.04 ± 0.02 Å
Fe5015	0.24 ± 0.05 Å
Mg ₁	-0.0004 ± 0.0005 mag
Mg ₂	0.0027 ± 0.0006 mag
Mg _b	-0.037 ± 0.025 Å
Fe5270	-0.01 ± 0.03 Å
Fe5335	0.01 ± 0.03 Å
Fe5406	-0.04 ± 0.03 Å
H δ_A	-0.43 ± 0.03 Å
H γ_A	-0.22 ± 0.04 Å
H δ_F	-0.25 ± 0.02 Å
H γ_F	-0.01 ± 0.02 Å

^a $EW_{S07} - EW_{This\ work}$

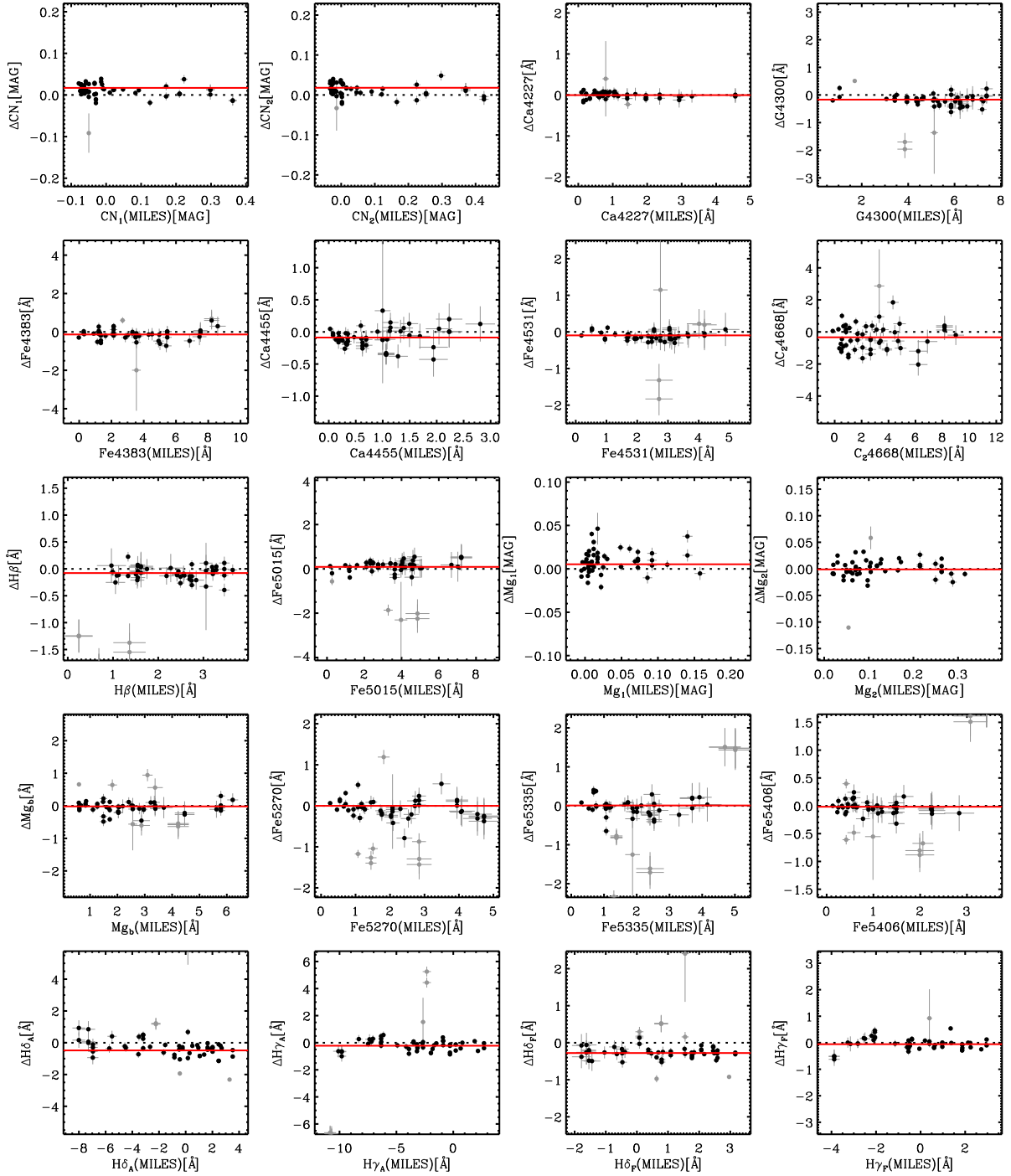


Fig. 7.— Comparison of 20 Lick index measurements on the LIS system for the calibration stars with the measurements on the MILES published spectra. The red solid lines represent the offsets between our data and the MILES data, which are determined by calculating the error-weighted mean values of the index measurement differences after removing outliers (gray dots) with three-sigma clipping.

Table 5. LIS index offsets between ours and the MILES data

Line Index	Δ_{LIS}^a
CN ₁	0.0170 ± 0.0004 mag
CN ₂	0.0180 ± 0.0006 mag
Ca4227	-0.00 ± 0.01 Å
G4300	-0.17 ± 0.02 Å
Fe4383	-0.13 ± 0.03 Å
Ca4455	-0.09 ± 0.01 Å
Fe4531	-0.09 ± 0.02 Å
C ₂ 4668	-0.34 ± 0.03 Å
H β	-0.08 ± 0.01 Å
Fe5015	0.09 ± 0.03 Å
Mg ₁	0.0053 ± 0.0003 mag
Mg ₂	-0.0010 ± 0.0004 mag
Mg _b	-0.018 ± 0.015 Å
Fe5270	-0.00 ± 0.02 Å
Fe5335	0.01 ± 0.02 Å
Fe5406	-0.02 ± 0.02 Å
H δ_A	-0.48 ± 0.02 Å
H γ_A	-0.22 ± 0.02 Å
H δ_F	-0.28 ± 0.01 Å
H γ_F	-0.05 ± 0.01 Å

^a $EW_{MILES} - EW_{This\ work}$

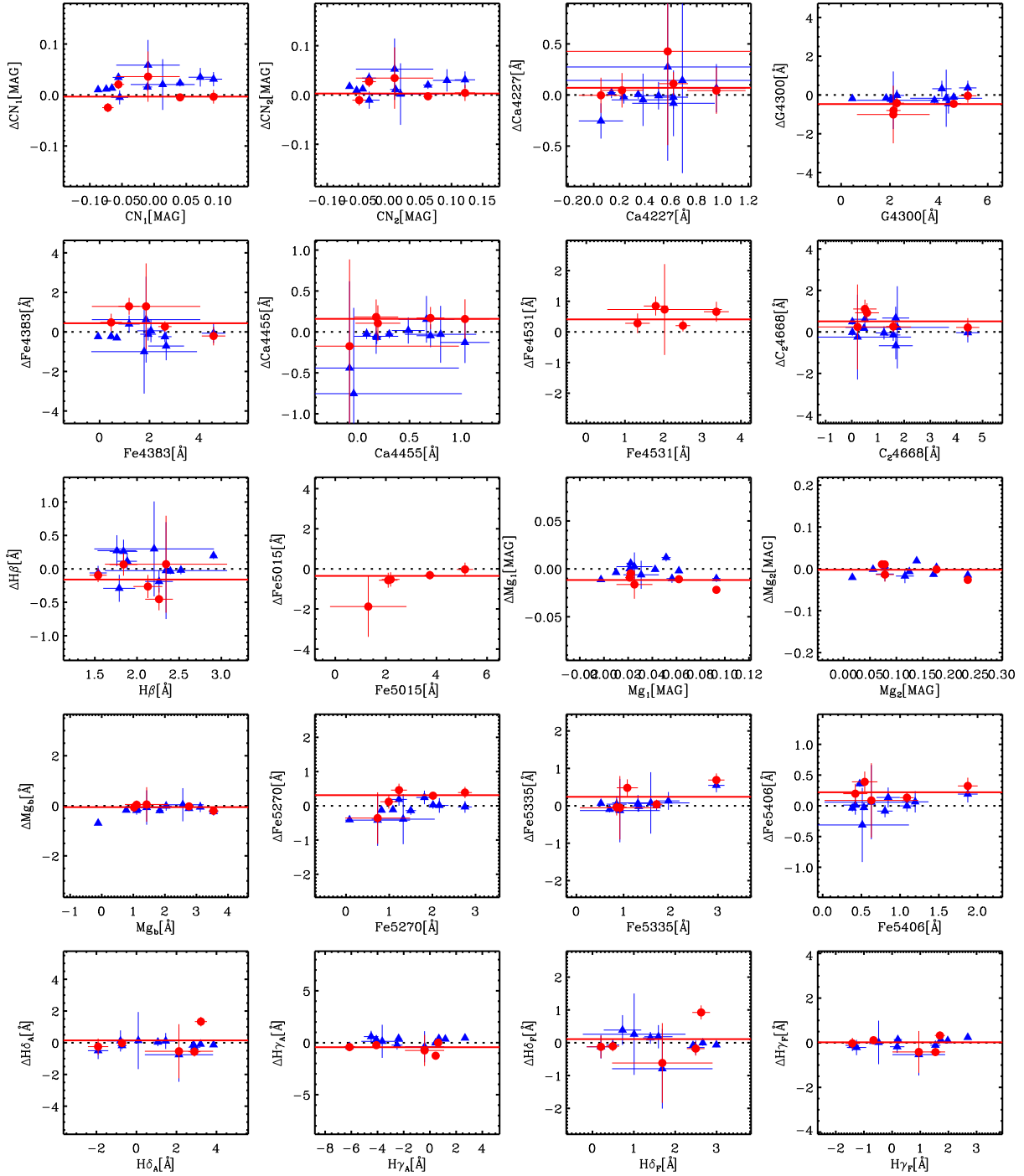


Fig. 8.— Comparison of Lick index measurements for GGCs with previous studies. The index measurements of this study are plotted along the horizontal axis and the differences between our index values and those from PSK02 (red filled circle) and from S12 (blue filled triangle) are plotted along the vertical axis. The zero-point offset between this study and PSK02 (red solid line) is determined by the error-weighted mean value of the difference.

Table 6. Lick index offsets against previous studies

Line Index	Δ_{PSK02}^a	Δ_{S12}^b
CN ₁	-0.0032 ± 0.0042 mag	0.0135 ± 0.0013 mag
CN ₂	0.0029 ± 0.0052 mag	0.0142 ± 0.0018 mag
Ca4227	0.07 ± 0.08 Å	0.00 ± 0.03 Å
G4300	-0.47 ± 0.13 Å	-0.19 ± 0.04 Å
Fe4383	0.44 ± 0.18 Å	-0.25 ± 0.07 Å
Ca4455	0.16 ± 0.09 Å	-0.03 ± 0.03 Å
Fe4531	0.4100 ± 0.1300 Å	NaN
C ₂ 4668	0.51 ± 0.19 Å	0.19 ± 0.07 Å
H β	-0.16 ± 0.07 Å	0.04 ± 0.03 Å
Fe5015	-0.3500 ± 0.1500 Å	NaN
Mg ₁	-0.0116 ± 0.0015 mag	-0.0040 ± 0.0006 mag
Mg ₂	-0.0021 ± 0.0018 mag	-0.0053 ± 0.0007 mag
Mg _b	-0.053 ± 0.070 Å	-0.142 ± 0.032 Å
Fe5270	0.31 ± 0.08 Å	-0.16 ± 0.03 Å
Fe5335	0.24 ± 0.09 Å	-0.03 ± 0.03 Å
Fe5406	0.22 ± 0.06 Å	-0.02 ± 0.03 Å
H δ_A	0.15 ± 0.15 Å	-0.12 ± 0.05 Å
H γ_A	-0.43 ± 0.14 Å	0.39 ± 0.05 Å
H δ_F	0.11 ± 0.10 Å	-0.07 ± 0.03 Å
H γ_F	0.02 ± 0.08 Å	0.13 ± 0.03 Å

^a $EW_{this\ work} - EW_{PSK02}$

^b $EW_{this\ work} - EW_{S12}$

Table 7. Metallicities, Lick/S07 indices, and their uncertainties for GGCs

ID	[Fe/H] (dex)	CN ₁ (mag)	CN ₂ (mag)	Ca4227 (Å)	G4300 (Å)	Fe4383 (Å)	Ca4455 (Å)	Fe4531 (Å)	C ₂ 4668 (Å)	H β (Å)	Fe5015 (Å)
NGC104	-0.76 0.02	0.0250 0.0010	0.0500 0.0010	0.56 0.01	4.66 0.02	2.49 0.03	0.67 0.02	1.68 0.03	1.60 0.01
NGC1851	-1.18 0.08	-0.0560 0.0010	-0.0310 0.0010	0.34 0.02	2.79 0.04	1.28 0.05	0.43 0.03	0.57 0.06	2.27 0.02
NGC1904	-1.58 0.02	-0.0850 0.0020	-0.0620 0.0020	0.21 0.04	1.89 0.06	0.70 0.09	0.23 0.05	-0.07 0.11	2.48 0.04
NGC2298	-1.96 0.04	-0.1020 0.0030	-0.0790 0.0040	0.24 0.06	1.66 0.10	0.65 0.14	0.15 0.07	0.17 0.16	2.68 0.06
NGC2808	-1.18 0.04	-0.0470 0.0040	-0.0240 0.0050	0.42 0.08	2.88 0.14	1.56 0.20	0.42 0.10	0.57 0.22	2.03 0.08
NGC3201	-1.51 0.02	-0.0870 0.0040	-0.0630 0.0050	0.36 0.08	2.30 0.40	1.35 0.19	0.39 0.10	-0.44 0.21	2.49 0.08
NGC5286	-1.70 0.07	-0.0860 0.0020	-0.0640 0.0030	0.23 0.04	2.08 0.07	0.76 0.11	0.23 0.06	0.03 0.12	2.44 0.05

Table 7—Continued

ID	[Fe/H]	CN ₁	CN ₂	Ca4227	G4300	Fe4383	Ca4455	Fe4531	C ₂ 4668	H β	Fe5015
	(dex)	(mag)	(mag)	(Å)	(Å)	(Å)	(Å)	(Å)	(Å)	(Å)	(Å)
NGC5904	-1.33	-0.0750	-0.0485	0.34	2.18	0.86	0.32	1.42	0.36	2.41	2.00
	0.02	0.0008	0.0014	0.02	0.03	0.05	0.02	0.06	0.06	0.02	0.08
NGC5927	-0.29	0.0799	0.1152	0.79	4.03	3.47	0.97	2.79	3.21	1.47	4.46
	0.07	0.0010	0.0013	0.02	0.03	0.05	0.03	0.05	0.07	0.03	0.07
NGC5946	-1.29	-0.0880	-0.0670	0.22	2.24	0.97	0.15	...	-0.37	2.44	...
	0.14	0.0030	0.0040	0.06	0.39	0.13	0.07	...	0.14	0.05	...
NGC5986	-1.63	-0.0850	-0.0620	0.27	1.81	0.90	0.19	...	0.01	2.50	...
	0.08	0.0010	0.0010	0.02	0.04	0.06	0.03	...	0.06	0.02	...
NGC6093	-1.75	-0.0660	-0.0435	0.24	2.01	0.38	0.18	0.93	-0.18	2.41	1.51
	0.08	0.0035	0.0043	0.07	0.12	0.18	0.09	0.13	0.20	0.07	0.16
NGC6121	-1.18	-0.0710	-0.0490	0.32	2.50	1.27	0.33	...	0.32	2.28	...
	0.02	0.0020	0.0020	0.04	0.06	0.09	0.05	...	0.10	0.04	...
NGC6171	-1.03	-0.0494	-0.0229	0.43	3.83	2.00	0.53	2.69	1.08	2.05	3.70
	0.02	0.0038	0.0048	0.08	0.11	0.16	0.09	0.37	0.17	0.07	0.37

Table 7—Continued

ID	[Fe/H]	CN ₁	CN ₂	Ca4227	G4300	Fe4383	Ca4455	Fe4531	C ₂ 4668	H β	Fe5015
	(dex)	(mag)	(mag)	(Å)	(Å)	(Å)	(Å)	(Å)	(Å)	(Å)	(Å)
NGC6205	-1.58	-0.0567	-0.0334	0.27	1.88	0.50	0.22	1.12	0.27	2.29	1.56
	0.04	0.0015	0.0018	0.03	0.05	0.08	0.04	0.06	0.09	0.03	0.07
NGC6218	-1.33	-0.0829	-0.0600	0.18	2.26	0.54	0.19	1.37	-0.10	2.48	2.36
	0.02	0.0006	0.0006	0.01	0.02	0.03	0.01	0.03	0.04	0.02	0.07
NGC6229	-1.43	-0.0557	-0.0279	0.38	2.30	0.84	0.33	1.62	0.71	2.33	2.31
	0.09	0.0042	0.0052	0.08	0.14	0.21	0.11	0.16	0.24	0.09	0.20
NGC6235	-1.38	-0.0600	-0.0350	0.34	2.76	1.58	0.37	...	0.90	2.26	...
	0.07	0.0010	0.0010	0.01	0.02	0.03	0.02	...	0.04	0.01	...
NGC6254	-1.57	-0.0800	-0.0580	0.27	2.34	1.03	0.24	...	-0.20	2.23	...
	0.02	0.0030	0.0040	0.05	0.09	0.12	0.06	...	0.12	0.05	...
NGC6266	-1.18	-0.0440	-0.0210	0.37	2.95	1.55	0.38	...	0.56	2.12	...
	0.07	0.0030	0.0040	0.06	0.10	0.13	0.07	...	0.14	0.05	...
NGC6284	-1.31	-0.0462	-0.0208	0.24	2.71	1.15	0.36	1.88	0.42	2.28	2.81
	0.09	0.0007	0.0008	0.02	0.02	0.04	0.02	0.04	0.06	0.02	0.07

Table 7—Continued

ID	[Fe/H]	CN ₁	CN ₂	Ca4227	G4300	Fe4383	Ca4455	Fe4531	C ₂ 4668	H β	Fe5015
	(dex)	(mag)	(mag)	(Å)	(Å)	(Å)	(Å)	(Å)	(Å)	(Å)	(Å)
NGC6304	-0.37	0.0371	0.0632	0.70	4.84	3.37	0.83	2.91	2.34	1.49	3.90
	0.07	0.0010	0.0020	0.03	0.05	0.07	0.04	0.47	0.08	0.03	0.45
NGC6316	-0.36	-0.0150	0.0070	0.61	4.48	2.69	0.66	...	1.16	1.50	...
	0.14	0.0030	0.0040	0.06	0.10	0.14	0.07	...	0.15	0.06	...
NGC6333	-1.79	-0.0930	-0.0700	0.22	1.59	0.68	0.19	...	-0.10	2.56	...
	0.09	0.0040	0.0050	0.08	0.12	0.17	0.09	...	0.18	0.07	...
NGC6341	-2.35	-0.0742	-0.0520	0.14	0.90	-0.04	0.08	0.57	0.10	2.70	0.70
	0.05	0.0015	0.0019	0.03	0.05	0.08	0.04	0.06	0.09	0.03	0.08
NGC6342	-0.49	-0.0072	0.0161	0.55	4.47	2.78	0.71	1.70	1.52	1.91	3.33
	0.14	0.0018	0.0019	0.03	0.05	0.08	0.04	1.45	0.09	0.03	1.44
NGC6352	-0.62	0.0020	0.0270	0.70	5.73	3.28	0.73	...	2.17	1.33	...
	0.05	0.0060	0.0070	0.11	0.18	0.25	0.13	...	0.26	0.10	...
NGC6356	-0.35	0.0397	0.0649	0.58	4.61	2.79	0.70	2.70	1.80	1.51	3.71
	0.14	0.0006	0.0007	0.01	0.02	0.03	0.01	0.03	0.04	0.02	0.04

Table 7—Continued

ID	[Fe/H]	CN ₁	CN ₂	Ca4227	G4300	Fe4383	Ca4455	Fe4531	C ₂ 4668	H β	Fe5015
	(dex)	(mag)	(mag)	(Å)	(Å)	(Å)	(Å)	(Å)	(Å)	(Å)	(Å)
NGC6362	-1.07	-0.0670	-0.0420	0.48	3.45	1.56	0.41	...	0.39	1.97	...
	0.05	0.0010	0.0010	0.02	0.03	0.04	0.02	...	0.04	0.02	...
NGC6388	-0.45	0.0409	0.0695	0.42	3.87	2.86	0.63	2.68	1.85	1.85	3.74
	0.04	0.0003	0.0004	0.01	0.01	0.02	0.01	0.01	0.02	0.01	0.02
NGC6441	-0.44	0.0447	0.0720	0.55	3.89	3.16	0.68	2.73	1.88	1.79	3.85
	0.07	0.0007	0.0008	0.01	0.02	0.03	0.02	0.03	0.04	0.02	0.06
NGC6517	-1.24	-0.0630	-0.0227	-0.13	1.54	0.89	-0.42	0.38	0.77	2.29	0.62
	0.14	0.0617	0.0783	1.15	1.86	2.52	1.22	1.64	2.04	0.65	1.24
NGC6522	-1.45	-0.0610	-0.0360	0.29	2.62	1.39	0.36	...	0.47	2.21	...
	0.08	0.0030	0.0040	0.07	0.11	0.15	0.08	...	0.15	0.06	...
NGC6528	0.07	0.0899	0.1178	0.97	4.77	5.14	1.05	3.13	4.66	1.61	4.82
	0.08	0.0011	0.0013	0.02	0.04	0.05	0.03	0.05	0.07	0.03	0.08
NGC6544	-1.47	-0.0560	-0.0380	0.34	2.90	1.47	0.40	...	0.33	1.60	...
	0.07	0.0050	0.0060	0.10	0.16	0.24	0.12	...	0.26	0.10	...

Table 7—Continued

ID	[Fe/H]	CN ₁	CN ₂	Ca4227	G4300	Fe4383	Ca4455	Fe4531	C ₂ 4668	H β	Fe5015
	(dex)	(mag)	(mag)	(Å)	(Å)	(Å)	(Å)	(Å)	(Å)	(Å)	(Å)
NGC6553	-0.16	0.1190	0.1484	1.10	4.92	4.35	0.98	3.49	3.99	1.67	5.38
	0.06	0.0016	0.0021	0.03	0.06	0.08	0.04	0.08	0.10	0.04	0.10
NGC6569	-0.72	-0.0440	-0.0200	0.51	3.81	1.91	0.48	...	0.99	1.74	...
	0.14	0.0020	0.0020	0.03	0.05	0.08	0.04	...	0.10	0.04	...
NGC6624	-0.42	0.0435	0.0731	0.56	4.45	2.85	0.68	2.69	1.92	1.56	3.84
	0.07	0.0005	0.0006	0.01	0.02	0.03	0.01	0.02	0.04	0.02	0.04
NGC6626	-1.46	-0.0538	-0.0324	0.24	2.56	1.13	0.30	1.71	0.48	2.28	2.83
	0.09	0.0005	0.0007	0.01	0.02	0.03	0.01	0.04	0.04	0.02	0.07
NGC6637	-0.59	0.0173	0.0402	0.49	4.73	2.48	0.62	2.59	1.78	1.50	3.60
	0.07	0.0004	0.0004	0.01	0.01	0.02	0.01	0.02	0.03	0.01	0.04
NGC6638	-0.99	-0.0257	-0.0009	0.51	4.09	2.06	0.47	1.98	1.28	1.77	3.11
	0.07	0.0010	0.0010	0.02	0.03	0.05	0.02	0.22	0.05	0.02	0.24
NGC6652	-0.76	-0.0400	-0.0170	0.43	4.34	1.97	0.48	...	1.06	2.03	...
	0.14	0.0030	0.0030	0.05	0.08	0.12	0.06	...	0.13	0.05	...

Table 7—Continued

ID	[Fe/H]	CN ₁	CN ₂	Ca4227	G4300	Fe4383	Ca4455	Fe4531	C ₂ 4668	H β	Fe5015
	(dex)	(mag)	(mag)	(Å)	(Å)	(Å)	(Å)	(Å)	(Å)	(Å)	(Å)
NGC6717	-1.26	-0.0446	-0.0155	0.56	3.21	1.73	0.67	2.48	1.56	1.86	3.72
	0.07	0.0068	0.0084	0.13	0.22	0.31	0.16	0.22	0.32	0.12	0.25
NGC6723	-1.10	-0.0570	-0.0330	0.30	3.06	1.29	0.32	...	0.34	2.14	...
	0.07	0.0040	0.0040	0.06	0.10	0.14	0.07	...	0.14	0.05	...
NGC6752	-1.55	-0.0850	-0.0610	0.20	1.99	0.66	0.22	...	0.08	2.59	...
	0.01	0.0040	0.0040	0.07	0.11	0.15	0.08	...	0.15	0.06	...
NGC6779	-2.00	-0.0749	-0.0514	0.23	1.34	0.82	-0.06	1.06	0.49	2.61	1.32
	0.09	0.0102	0.0128	0.19	0.34	0.50	0.25	0.37	0.52	0.19	0.41
NGC6838	-0.82	-0.0282	-0.0049	0.74	4.41	2.08	0.84	2.18	1.67	1.35	3.20
	0.02	0.0067	0.0083	0.12	0.21	0.29	0.15	0.21	0.29	0.11	0.23
NGC6864	-1.29	-0.0471	-0.0218	0.41	2.71	1.27	0.36	1.83	0.96	2.19	2.62
	0.14	0.0029	0.0036	0.06	0.10	0.14	0.07	0.11	0.16	0.06	0.13
NGC6934	-1.56	-0.0668	-0.0399	0.34	2.02	0.48	0.20	1.25	0.57	2.59	1.97
	0.09	0.0041	0.0050	0.08	0.14	0.21	0.11	0.16	0.23	0.08	0.19

Table 7—Continued

ID	[Fe/H]	CN ₁	CN ₂	Ca4227	G4300	Fe4383	Ca4455	Fe4531	C ₂ 4668	H β	Fe5015
	(dex)	(mag)	(mag)	(Å)	(Å)	(Å)	(Å)	(Å)	(Å)	(Å)	(Å)
NGC6981	-1.48	-0.0504	-0.0352	0.24	2.47	0.42	0.24	1.46	0.18	2.23	2.30
	0.07	0.0006	0.0007	0.01	0.02	0.04	0.02	0.03	0.06	0.03	0.06
NGC7006	-1.46	-0.0671	-0.0435	0.34	2.17	0.85	0.24	1.32	0.47	2.55	1.92
	0.06	0.0086	0.0107	0.16	0.29	0.43	0.22	0.32	0.47	0.17	0.38
NGC7078	-2.33	-0.0904	-0.0700	0.13	0.54	0.06	0.10	0.38	-0.25	2.80	0.56
	0.02	0.0014	0.0016	0.03	0.04	0.06	0.03	0.07	0.07	0.03	0.09
NGC7089	-1.66	-0.0770	-0.0546	0.24	1.89	0.53	0.20	1.10	0.03	2.53	1.52
	0.07	0.0014	0.0018	0.03	0.05	0.07	0.04	0.07	0.08	0.03	0.08

Table 7. Metallicities, Lick/S07 indices, and their uncertainties for GGCs, continued.

ID	Mg ₁	Mg ₂	Mgb	Fe5270	Fe5335	Fe5406	H δ_A	H γ_A	H δ_F	H γ_F	Source ^a
	(mag)	(mag)	(Å)	(Å)	(Å)	(Å)	(Å)	(Å)	(Å)	(Å)	
NGC104	0.0569	0.1589	2.690	1.91	1.68	1.06	-0.48	-4.27	0.68	-0.66	2
	0.0003	0.0004	0.010	0.02	0.02	0.01	0.02	0.02	0.02	0.01	
NGC1851	0.0251	0.0829	1.350	1.40	1.12	0.67	2.23	-0.60	2.06	1.23	2
	0.0005	0.0006	0.020	0.03	0.03	0.02	0.04	0.03	0.02	0.02	
NGC1904	0.0103	0.0485	0.830	0.93	0.78	0.34	3.17	0.87	2.61	1.88	2
	0.0009	0.0011	0.050	0.05	0.06	0.04	0.06	0.06	0.04	0.04	
NGC2298	0.0070	0.0442	0.790	0.74	0.63	0.24	3.70	1.45	2.87	2.13	2
	0.0013	0.0016	0.070	0.07	0.08	0.06	0.09	0.09	0.07	0.06	
NGC2808	0.0231	0.0844	1.330	1.41	1.16	0.70	1.57	-1.28	1.65	0.83	2
	0.0018	0.0021	0.090	0.10	0.11	0.08	0.14	0.13	0.10	0.08	
NGC3201	0.0079	0.0617	1.140	1.09	0.89	0.58	2.77	-0.04	2.27	1.41	2
	0.0017	0.0019	0.080	0.09	0.10	0.07	0.13	0.29	0.09	0.12	
NGC5286	0.0149	0.0585	0.960	0.92	0.80	0.38	3.27	0.65	2.57	1.75	2
	0.0010	0.0012	0.050	0.05	0.06	0.05	0.07	0.07	0.05	0.04	

Table 7—Continued

ID	Mg ₁	Mg ₂	Mgb	Fe5270	Fe5335	Fe5406	H δ_A	H γ_A	H δ_F	H γ_F	Source ^a
	(mag)	(mag)	(Å)	(Å)	(Å)	(Å)	(Å)	(Å)	(Å)	(Å)	
NGC5904	0.0213	0.0766	1.199	1.16	0.97	0.55	2.91	0.43	2.48	1.66	1,2
	0.0005	0.0006	0.023	0.02	0.03	0.02	0.04	0.03	0.02	0.02	
NGC5927	0.0737	0.2152	3.500	2.50	2.04	1.36	-1.71	-4.60	0.20	-1.04	2,3
	0.0007	0.0009	0.033	0.04	0.04	0.03	0.04	0.04	0.03	0.03	
NGC5946	0.0243	0.0649	0.890	0.97	0.64	0.37	3.29	0.42	2.58	1.70	2
	0.0011	0.0013	0.050	0.06	0.07	0.05	0.10	0.28	0.07	0.10	
NGC5986	0.0129	0.0572	0.920	0.89	0.72	0.39	3.25	0.80	2.66	1.88	2
	0.0005	0.0006	0.020	0.03	0.03	0.02	0.04	0.04	0.03	0.02	
NGC6093	0.0090	0.0484	0.683	0.78	0.66	0.34	3.16	0.95	2.61	1.82	1
	0.0016	0.0018	0.075	0.08	0.10	0.07	0.12	0.11	0.08	0.07	
NGC6121	0.0245	0.0883	1.580	1.21	0.98	0.57	2.85	0.00	2.34	1.40	2
	0.0008	0.0010	0.040	0.05	0.05	0.04	0.06	0.06	0.04	0.04	
NGC6171	0.0410	0.1213	2.049	1.60	1.25	0.73	1.36	-2.30	1.42	0.34	1,2
	0.0013	0.0015	0.057	0.07	0.07	0.06	0.13	0.12	0.10	0.08	

Table 7—Continued

ID	Mg ₁	Mg ₂	Mgb	Fe5270	Fe5335	Fe5406	H δ_A	H γ_A	H δ_F	H γ_F	Source ^a
	(mag)	(mag)	(Å)	(Å)	(Å)	(Å)	(Å)	(Å)	(Å)	(Å)	
NGC6205	0.0081	0.0561	0.660	1.13	0.79	0.58	2.39	0.81	2.16	1.77	1
	0.0008	0.0009	0.036	0.04	0.05	0.03	0.05	0.05	0.04	0.03	
NGC6218	0.0160	0.0694	1.221	1.05	0.86	0.42	3.50	0.92	2.75	1.86	1,2,3
	0.0003	0.0004	0.017	0.02	0.02	0.02	0.02	0.02	0.01	0.01	
NGC6229	0.0219	0.0836	1.233	1.32	1.11	0.57	2.79	0.32	2.40	1.59	1
	0.0020	0.0023	0.095	0.11	0.12	0.09	0.14	0.14	0.10	0.09	
NGC6235	0.0244	0.0862	1.160	1.41	1.18	0.66	2.83	-0.77	2.35	1.17	2
	0.0003	0.0004	0.010	0.02	0.02	0.01	0.02	0.02	0.01	0.01	
NGC6254	0.0135	0.0594	0.900	0.95	0.76	0.36	2.78	-0.05	2.26	1.40	2
	0.0009	0.0011	0.040	0.05	0.05	0.04	0.11	0.09	0.07	0.06	
NGC6266	0.0240	0.0902	1.540	1.34	1.12	0.64	1.88	-0.96	1.88	1.00	2
	0.0011	0.0013	0.050	0.05	0.06	0.04	0.12	0.11	0.09	0.07	
NGC6284	0.0293	0.0939	1.447	1.22	1.15	0.67	2.50	-0.08	2.58	1.42	2,3
	0.0006	0.0007	0.024	0.03	0.03	0.02	0.02	0.03	0.02	0.02	

Table 7—Continued

ID	Mg ₁ (mag)	Mg ₂ (mag)	Mgb (Å)	Fe5270 (Å)	Fe5335 (Å)	Fe5406 (Å)	Hδ _A (Å)	Hγ _A (Å)	Hδ _F (Å)	Hγ _F (Å)	Source ^a
NGC6304	0.0662	0.1833	3.169	2.15	1.82	1.13	-0.91	-5.08	0.34	-1.05	1,2
	0.0006	0.0007	0.030	0.03	0.04	0.03	0.05	0.04	0.03	0.03	
NGC6316	0.0544	0.1547	2.540	1.83	1.44	0.96	0.10	-3.97	0.80	-0.57	2
	0.0011	0.0013	0.050	0.06	0.07	0.05	0.11	0.10	0.08	0.06	
NGC6333	0.0149	0.0500	0.780	0.78	0.60	0.33	3.57	1.15	2.78	1.99	2
	0.0013	0.0016	0.060	0.07	0.08	0.06	0.14	0.13	0.10	0.08	
NGC6341	0.0030	0.0270	0.016	0.47	0.65	0.46	3.40	2.11	2.74	2.35	1
	0.0008	0.0009	0.039	0.04	0.05	0.04	0.05	0.05	0.03	0.03	
NGC6342	0.0370	0.1333	2.525	1.71	1.50	0.82	-0.05	-3.78	0.75	-0.49	1,2
	0.0007	0.0008	0.033	0.03	0.04	0.03	0.06	0.05	0.04	0.04	
NGC6352	0.0548	0.1607	2.920	1.85	1.71	1.17	-0.15	-5.38	0.78	-1.25	2
	0.0020	0.0024	0.100	0.11	0.12	0.09	0.19	0.18	0.14	0.11	
NGC6356	0.0623	0.1742	2.780	2.01	1.82	1.15	-0.55	-4.30	0.70	-0.74	1,2,3
	0.0004	0.0004	0.017	0.02	0.02	0.02	0.02	0.02	0.01	0.01	

Table 7—Continued

ID	Mg ₁ (mag)	Mg ₂ (mag)	Mgb (Å)	Fe5270 (Å)	Fe5335 (Å)	Fe5406 (Å)	H δ_A (Å)	H γ_A (Å)	H δ_F (Å)	H γ_F (Å)	Source ^a
NGC6362	0.0322	0.1098	1.940	1.37	1.03	0.68	1.74	-1.64	1.64	0.58	2
	0.0003	0.0004	0.020	0.02	0.02	0.01	0.03	0.03	0.02	0.02	
NGC6388	0.0454	0.1436	2.112	2.18	1.90	1.23	0.28	-3.05	1.12	0.04	2,3
	0.0002	0.0003	0.011	0.01	0.01	0.01	0.01	0.01	0.01	0.01	
NGC6441	0.0603	0.1680	2.657	2.18	1.85	1.20	0.25	-3.29	1.14	-0.04	2,3
	0.0004	0.0005	0.018	0.02	0.02	0.02	0.02	0.02	0.02	0.02	
NGC6517	0.0017	0.0477	0.521	0.83	0.76	0.26	2.84	0.53	2.60	1.41	1
	0.0118	0.0127	0.527	0.55	0.60	0.43	2.17	1.73	1.53	1.08	
NGC6522	0.0394	0.1040	1.480	1.41	1.11	0.68	2.79	-0.37	2.39	1.33	2
	0.0012	0.0014	0.050	0.06	0.07	0.05	0.12	0.11	0.09	0.07	
NGC6528	0.1027	0.2555	3.711	2.72	2.51	1.74	-1.51	-6.09	0.43	-1.35	1,2,3
	0.0007	0.0008	0.032	0.03	0.03	0.03	0.04	0.04	0.03	0.03	
NGC6544	0.0413	0.0934	1.000	1.37	1.07	0.65	1.85	-1.48	1.49	0.53	2
	0.0020	0.0024	0.090	0.10	0.12	0.09	0.19	0.17	0.13	0.11	

Table 7—Continued

ID	Mg ₁ (mag)	Mg ₂ (mag)	Mgb (Å)	Fe5270 (Å)	Fe5335 (Å)	Fe5406 (Å)	Hδ _A (Å)	Hγ _A (Å)	Hδ _F (Å)	Hγ _F (Å)	Source ^a
NGC6553	0.0909	0.2489	3.835	2.85	2.40	1.55	-1.56	-6.12	0.83	-1.31	2,3
	0.0009	0.0011	0.042	0.05	0.05	0.04	0.06	0.06	0.04	0.04	
NGC6569	0.0454	0.1341	2.140	1.50	1.30	0.81	0.95	-2.60	1.12	0.10	2
	0.0008	0.0010	0.040	0.04	0.05	0.04	0.06	0.06	0.04	0.04	
NGC6624	0.0572	0.1643	2.645	2.06	1.76	1.12	-0.42	-4.12	0.72	-0.57	2,3
	0.0003	0.0004	0.014	0.02	0.02	0.02	0.02	0.02	0.01	0.01	
NGC6626	0.0251	0.0904	1.438	1.21	1.09	0.63	2.84	-0.06	2.44	1.42	1,2,3
	0.0003	0.0003	0.017	0.02	0.02	0.02	0.02	0.02	0.01	0.01	
NGC6637	0.0469	0.1524	2.498	1.85	1.58	1.01	-0.51	-4.28	0.51	-0.79	2,3
	0.0003	0.0004	0.013	0.01	0.02	0.01	0.01	0.02	0.01	0.01	
NGC6638	0.0429	0.1309	2.024	1.64	1.34	0.89	1.03	-2.79	1.25	0.06	1,2
	0.0004	0.0005	0.020	0.02	0.02	0.02	0.04	0.03	0.03	0.02	
NGC6652	0.0253	0.1080	2.060	1.50	1.27	0.68	1.10	-2.70	1.37	0.05	2
	0.0011	0.0013	0.050	0.06	0.07	0.05	0.08	0.08	0.06	0.05	

Table 7—Continued

ID	Mg ₁	Mg ₂	Mgb	Fe5270	Fe5335	Fe5406	H δ_A	H γ_A	H δ_F	H γ_F	Source ^a
	(mag)	(mag)	(Å)	(Å)	(Å)	(Å)	(Å)	(Å)	(Å)	(Å)	
NGC6717	0.0640	0.1443	1.573	2.08	1.81	1.25	2.82	-0.97	2.40	1.11	1
	0.0025	0.0029	0.120	0.13	0.14	0.10	0.23	0.22	0.16	0.13	
NGC6723	0.0188	0.0830	1.460	1.17	0.91	0.53	2.02	-0.96	1.88	0.97	2
	0.0011	0.0013	0.050	0.05	0.06	0.04	0.13	0.11	0.09	0.07	
NGC6752	0.0109	0.0535	0.940	0.87	0.74	0.32	3.22	0.91	2.69	1.93	2
	0.0012	0.0014	0.060	0.06	0.07	0.05	0.14	0.12	0.09	0.07	
NGC6779	0.0099	0.0443	0.406	0.82	0.49	0.27	3.67	1.75	2.85	2.33	1
	0.0041	0.0047	0.197	0.21	0.25	0.18	0.34	0.32	0.24	0.20	
NGC6838	0.0642	0.1609	2.443	1.90	1.58	1.05	0.33	-4.01	0.94	-0.77	1
	0.0023	0.0027	0.108	0.12	0.13	0.10	0.24	0.22	0.17	0.14	
NGC6864	0.0207	0.0850	1.224	1.48	1.20	0.73	2.19	-0.42	2.01	1.30	1
	0.0013	0.0015	0.062	0.07	0.08	0.06	0.10	0.10	0.07	0.06	
NGC6934	0.0087	0.0479	0.211	1.03	0.61	0.79	2.79	0.81	2.35	1.80	1
	0.0019	0.0022	0.092	0.10	0.12	0.08	0.14	0.13	0.10	0.08	

Table 7—Continued

ID	Mg ₁ (mag)	Mg ₂ (mag)	Mgb (Å)	Fe5270 (Å)	Fe5335 (Å)	Fe5406 (Å)	H δ_A (Å)	H γ_A (Å)	H δ_F (Å)	H γ_F (Å)	Source ^a
NGC6981	0.0190	0.0601	1.031	1.17	0.85	0.38	2.05	0.21	1.81	1.40	1,3
	0.0007	0.0008	0.031	0.04	0.04	0.03	0.02	0.02	0.01	0.02	
NGC7006	0.0077	0.0489	0.101	0.82	0.58	0.70	2.63	0.53	2.31	1.70	1
	0.0039	0.0045	0.190	0.21	0.24	0.17	0.29	0.28	0.21	0.18	
NGC7078	0.0039	0.0276	0.331	0.34	0.48	0.24	3.89	2.52	3.01	2.60	1,2
	0.0006	0.0007	0.025	0.03	0.03	0.02	0.05	0.04	0.03	0.03	
NGC7089	0.0115	0.0562	0.843	0.88	0.74	0.40	3.22	1.10	2.67	1.95	1,2
	0.0006	0.0007	0.031	0.03	0.04	0.03	0.05	0.05	0.03	0.03	

Note. — (a) Sources of Lick indices: 1 = this work; 2 = S12; 3 = PSK02 (calibrated to this work)

Table 8. Metallicities, LIS indices, and their uncertainties for GGCs

ID	[Fe/H] (dex)	CN ₁ (mag)	CN ₂ (mag)	Ca4227 (Å)	G4300 (Å)	Fe4383 (Å)	Ca4455 (Å)	Fe4531 (Å)	C ₂ 4668 (Å)	H β (Å)	Fe5015 (Å)
NGC104	-0.76 0.02	0.0520 0.0010	0.0931 0.0020	0.82 0.03	4.78 0.05	2.76 0.07	0.77 0.04	1.75 0.08	1.56 0.03
NGC1851	-1.18 0.08	-0.0320 0.0020	0.0111 0.0030	0.46 0.04	2.92 0.08	1.27 0.11	0.47 0.06	0.56 0.13	2.27 0.05
NGC1904	-1.58 0.02	-0.0620 0.0017	-0.0209 0.0024	0.26 0.04	1.97 0.06	0.59 0.09	0.21 0.05	-0.15 0.11	2.49 0.04
NGC2298	-1.96 0.04	-0.0809 0.0048	-0.0379 0.0057	0.27 0.09	1.68 0.17	0.47 0.24	0.14 0.12	0.10 0.28	2.69 0.10
NGC2808	-1.18 0.04	-0.0214 0.0017	0.0189 0.0017	0.57 0.02	2.97 0.04	1.57 0.06	0.47 0.03	0.58 0.07	2.01 0.03
NGC3201	-1.51 0.02	-0.0650 0.0028	-0.0214 0.0035	0.47 0.06	2.46 0.10	1.32 0.15	0.44 0.07	-0.50 0.16	2.51 0.06
NGC5286	-1.70 0.07	-0.0621 0.0013	-0.0213 0.0016	0.30 0.03	2.17 0.05	0.67 0.07	0.22 0.04	0.03 0.08	2.43 0.03

Table 8—Continued

ID	[Fe/H]	CN ₁	CN ₂	Ca4227	G4300	Fe4383	Ca4455	Fe4531	C ₂ 4668	H β	Fe5015
	(dex)	(mag)	(mag)	(Å)	(Å)	(Å)	(Å)	(Å)	(Å)	(Å)	(Å)
NGC5904	-1.33	-0.0542	-0.0119	0.45	2.38	0.97	0.35	1.50	0.28	2.42	2.08
	0.02	0.0009	0.0014	0.02	0.04	0.05	0.03	2.09	0.06	0.02	2.68
NGC5927	-0.29	0.0670	0.1081	1.04	4.92	3.95	1.14	...	2.73	1.38	...
	0.07	0.0035	0.0040	0.06	0.11	0.14	0.07	...	0.15	0.06	...
NGC5946	-1.29	-0.0660	-0.0259	0.28	2.32	0.82	0.14	...	-0.40	2.43	...
	0.14	0.0080	0.0090	0.15	0.26	0.38	0.19	...	0.40	0.14	...
NGC5986	-1.63	-0.0630	-0.0209	0.35	1.89	0.78	0.16	...	-0.03	2.50	...
	0.08	0.0030	0.0030	0.06	0.10	0.15	0.08	...	0.17	0.06	...
NGC6093	-1.75	-0.0566	-0.0169	0.30	2.27	0.49	0.16	0.96	-0.40	2.41	1.50
	0.08	0.0604	0.0708	1.17	2.13	3.14	1.60	2.44	3.63	1.38	3.04
NGC6121	-1.18	-0.0480	-0.0089	0.41	2.58	1.26	0.35	...	0.33	2.28	...
	0.02	0.0030	0.0030	0.05	0.09	0.13	0.07	...	0.15	0.05	...
NGC6171	-1.03	-0.0235	0.0201	0.57	3.96	2.15	0.59	2.88	1.06	2.07	3.94
	0.02	0.0057	0.0064	0.10	0.18	0.25	0.12	6.57	0.26	0.10	8.44

Table 8—Continued

ID	[Fe/H]	CN ₁	CN ₂	Ca4227	G4300	Fe4383	Ca4455	Fe4531	C ₂ 4668	H β	Fe5015
	(dex)	(mag)	(mag)	(Å)	(Å)	(Å)	(Å)	(Å)	(Å)	(Å)	(Å)
NGC6205	-1.58	-0.0473	-0.0078	0.34	2.10	0.68	0.20	1.16	0.06	2.29	1.57
	0.04	0.0657	0.0776	1.29	2.36	3.51	1.81	2.78	4.18	1.62	3.63
NGC6218	-1.33	-0.0679	-0.0239	0.39	2.40	0.75	0.21	1.86	-0.13	2.46	2.29
	0.02	0.0040	0.0050	0.08	0.14	0.20	0.10	6.18	0.23	0.08	8.24
NGC6229	-1.43	-0.0448	0.0012	0.50	2.55	1.07	0.34	1.68	0.52	2.32	2.39
	0.09	0.0676	0.0796	1.32	2.41	3.58	1.84	2.81	4.23	1.64	3.61
NGC6235	-1.38	-0.0360	0.0071	0.49	2.90	1.68	0.40	...	0.93	2.25	...
	0.07	0.0100	0.0120	0.19	0.34	0.47	0.23	...	0.51	0.18	...
NGC6254	-1.57	-0.0570	-0.0179	0.34	2.44	0.91	0.23	...	-0.24	2.22	...
	0.02	0.0030	0.0030	0.05	0.09	0.13	0.07	...	0.15	0.05	...
NGC6266	-1.18	-0.0210	0.0201	0.50	3.07	1.60	0.44	...	0.58	2.10	...
	0.07	0.0020	0.0020	0.03	0.06	0.08	0.04	...	0.09	0.03	...
NGC6284	-1.31	-0.0358	0.0071	0.48	2.69	1.38	0.41	...	0.50	2.28	...
	0.09	0.0024	0.0028	0.05	0.08	0.12	0.06	...	0.14	0.05	...

Table 8—Continued

ID	[Fe/H]	CN ₁	CN ₂	Ca4227	G4300	Fe4383	Ca4455	Fe4531	C ₂ 4668	H β	Fe5015
	(dex)	(mag)	(mag)	(Å)	(Å)	(Å)	(Å)	(Å)	(Å)	(Å)	(Å)
NGC6304	-0.37	0.0641	0.1041	0.98	4.97	3.69	1.01	3.20	2.41	1.47	4.26
	0.07	0.0050	0.0060	0.10	0.16	0.22	0.11	4.67	0.24	0.09	5.82
NGC6316	-0.36	0.0107	0.0478	0.82	4.62	2.87	0.81	...	1.20	1.47	...
	0.14	0.0046	0.0053	0.08	0.14	0.19	0.10	...	0.20	0.07	...
NGC6333	-1.79	-0.0700	-0.0289	0.29	1.67	0.53	0.17	...	-0.13	2.56	...
	0.09	0.0030	0.0040	0.06	0.11	0.16	0.08	...	0.19	0.07	...
NGC6341	-2.35	-0.0654	-0.0262	0.15	1.09	0.00	0.02	0.58	-0.14	2.73	0.54
	0.05	0.0367	0.0431	0.72	1.32	1.97	1.01	1.57	2.35	0.90	2.04
NGC6342	-0.49	0.0146	0.0504	0.70	4.54	2.99	0.83	1.83	1.49	1.93	3.67
	0.14	0.0070	0.0079	0.13	0.22	0.31	0.15	5.75	0.33	0.12	7.39
NGC6352	-0.62	0.0280	0.0671	0.93	5.77	3.57	0.90	...	2.24	1.32	...
	0.05	0.0060	0.0070	0.12	0.20	0.28	0.14	...	0.30	0.11	...
NGC6356	-0.35	0.0431	0.0831	0.89	4.85	3.11	0.90	2.69	1.78	1.58	4.01
	0.14	0.0040	0.0040	0.07	0.11	0.16	0.08	3.58	0.18	0.07	4.43

Table 8—Continued

ID	[Fe/H]	CN ₁	CN ₂	Ca4227	G4300	Fe4383	Ca4455	Fe4531	C ₂ 4668	H β	Fe5015
	(dex)	(mag)	(mag)	(Å)	(Å)	(Å)	(Å)	(Å)	(Å)	(Å)	(Å)
NGC6362	-1.07	-0.0430	0.0001	0.63	3.55	1.69	0.45	...	0.45	1.97	...
	0.05	0.0040	0.0050	0.08	0.14	0.21	0.10	...	0.23	0.08	...
NGC6388	-0.45	0.0450	0.0871	0.71	4.16	3.19	0.88	...	1.96	1.86	...
	0.04	0.0020	0.0020	0.04	0.06	0.09	0.05	...	0.10	0.04	...
NGC6441	-0.44	0.0470	0.0896	0.80	4.14	3.30	0.93	...	1.98	1.79	...
	0.07	0.0014	0.0021	0.03	0.05	0.07	0.04	...	0.08	0.03	...
NGC6517	-1.24	-0.0581	0.0009	-0.19	1.63	0.77	-0.47	0.28	0.58	2.23	0.53
	0.14	0.1166	0.1390	2.36	4.34	6.37	3.39	5.26	7.98	3.08	6.73
NGC6522	-1.45	-0.0370	0.0071	0.37	2.74	1.36	0.42	...	0.50	2.20	...
	0.08	0.0040	0.0040	0.07	0.12	0.18	0.09	...	0.19	0.07	...
NGC6528	0.07	0.0897	0.1354	1.27	4.90	5.06	1.45	3.58	4.60	1.56	5.55
	0.08	0.0026	0.0031	0.05	0.08	0.10	0.05	3.71	0.11	0.04	4.33
NGC6544	-1.47	-0.0330	-0.0009	0.44	2.96	1.42	0.45	...	0.35	1.57	...
	0.07	0.0070	0.0080	0.13	0.22	0.31	0.15	...	0.32	0.12	...

Table 8—Continued

ID	[Fe/H]	CN ₁	CN ₂	Ca4227	G4300	Fe4383	Ca4455	Fe4531	C ₂ 4668	H β	Fe5015
	(dex)	(mag)	(mag)	(Å)	(Å)	(Å)	(Å)	(Å)	(Å)	(Å)	(Å)
NGC6553	-0.16	0.0690	0.1111	1.00	4.74	4.16	1.15	...	4.05	1.51	...
	0.06	0.0070	0.0090	0.13	0.24	0.31	0.16	...	0.31	0.11	...
NGC6569	-0.72	-0.0190	0.0211	0.69	3.91	1.96	0.54	...	0.98	1.72	...
	0.14	0.0080	0.0090	0.14	0.25	0.34	0.17	...	0.35	0.13	...
NGC6624	-0.42	0.0458	0.0866	0.76	4.75	3.17	0.94	...	1.82	1.63	...
	0.07	0.0017	0.0021	0.03	0.05	0.08	0.04	...	0.09	0.04	...
NGC6626	-1.46	-0.0450	-0.0019	0.39	2.52	1.19	0.40	2.17	0.48	2.36	1.30
	0.09	0.0030	0.0030	0.05	0.09	0.13	0.07	9.73	0.15	0.05	13.10
NGC6637	-0.59	0.0170	0.0551	0.81	4.92	2.61	0.81	...	1.73	1.54	...
	0.07	0.0030	0.0030	0.05	0.09	0.13	0.06	...	0.14	0.05	...
NGC6638	-0.99	-0.0020	0.0401	0.67	4.25	2.19	0.55	2.12	1.33	1.76	3.31
	0.07	0.0040	0.0050	0.08	0.14	0.20	0.10	4.34	0.22	0.08	5.29
NGC6652	-0.76	-0.0155	0.0231	0.58	4.49	2.18	0.56	...	1.09	2.00	...
	0.14	0.0021	0.0028	0.04	0.07	0.11	0.06	...	0.13	0.05	...

Table 8—Continued

ID	[Fe/H]	CN ₁	CN ₂	Ca4227	G4300	Fe4383	Ca4455	Fe4531	C ₂ 4668	H β	Fe5015
	(dex)	(mag)	(mag)	(Å)	(Å)	(Å)	(Å)	(Å)	(Å)	(Å)	(Å)
NGC6717	-1.26	-0.0405	0.0077	0.75	3.47	2.00	0.77	2.57	1.40	1.88	3.95
	0.07	0.0806	0.0947	1.56	2.83	4.10	2.08	3.13	4.61	1.76	3.76
NGC6723	-1.10	-0.0340	0.0081	0.40	3.18	1.37	0.36	...	0.35	2.13	...
	0.07	0.0040	0.0040	0.07	0.12	0.17	0.09	...	0.20	0.08	...
NGC6752	-1.55	-0.0620	-0.0189	0.25	2.10	0.56	0.20	...	0.07	2.59	...
	0.01	0.0020	0.0020	0.04	0.07	0.10	0.05	...	0.12	0.05	...
NGC6779	-2.00	-0.0607	-0.0152	0.26	1.56	0.70	-0.19	1.08	0.43	2.62	1.28
	0.09	0.1338	0.1586	2.68	4.93	7.36	3.86	6.04	9.14	3.58	7.96
NGC6838	-0.82	-0.0149	0.0216	1.01	4.67	2.62	1.01	2.35	1.57	1.33	3.48
	0.02	0.1335	0.1589	2.64	4.84	7.17	3.69	5.67	8.56	3.37	7.35
NGC6864	-1.29	-0.0365	0.0057	0.56	2.98	1.53	0.41	1.94	0.81	2.17	2.78
	0.14	0.0477	0.0561	0.92	1.66	2.43	1.24	1.87	2.79	1.07	2.31
NGC6934	-1.56	-0.0570	-0.0133	0.43	2.23	0.65	0.20	1.31	0.39	2.61	2.04
	0.09	0.0816	0.0961	1.60	2.92	4.33	2.25	3.44	5.17	2.00	4.44

Table 8—Continued

ID	[Fe/H]	CN ₁	CN ₂	Ca4227	G4300	Fe4383	Ca4455	Fe4531	C ₂ 4668	H β	Fe5015
	(dex)	(mag)	(mag)	(Å)	(Å)	(Å)	(Å)	(Å)	(Å)	(Å)	(Å)
NGC6981	-1.48	-0.0619	-0.0197	0.24	2.37	0.68	0.19	1.33	0.40	2.13	2.17
	0.07	0.1400	0.1661	2.79	5.13	7.68	4.04	6.31	9.62	3.79	8.47
NGC7006	-1.46	-0.0590	-0.0180	0.40	2.35	1.02	0.21	1.35	0.25	2.58	1.97
	0.06	0.1205	0.1427	2.41	4.41	6.58	3.44	5.37	8.14	3.17	7.11
NGC7078	-2.33	-0.0762	-0.0388	0.13	0.71	-0.05	0.03	0.35	-0.51	2.71	0.36
	0.02	0.0017	0.0017	0.03	0.05	0.08	0.04	0.91	0.09	0.03	1.19
NGC7089	-1.66	-0.0630	-0.0199	0.32	2.12	0.58	0.22	1.15	0.03	2.54	1.55
	0.07	0.0020	0.0030	0.04	0.08	0.12	0.06	1.88	0.14	0.05	2.42

Table 8. Metallicities, LIS indices, and their uncertainties for GGCs, continued.

ID	Mg ₁	Mg ₂	Mgb	Fe5270	Fe5335	Fe5406	H δ_A	H γ_A	H δ_F	H γ_F	Source ^a
	(mag)	(mag)	(Å)	(Å)	(Å)	(Å)	(Å)	(Å)	(Å)	(Å)	
NGC104	0.0596	0.1515	2.540	1.99	1.96	1.29	-0.93	-3.86	0.69	-0.62	2
	0.0010	0.0010	0.030	0.03	0.04	0.03	0.05	0.05	0.04	0.03	
NGC1851	0.0276	0.0755	1.140	1.44	1.34	0.85	1.94	-0.27	2.11	1.35	2
	0.0010	0.0010	0.054	0.06	0.07	0.05	0.08	0.08	0.05	0.05	
NGC1904	0.0118	0.0405	0.622	0.92	0.92	0.49	2.96	1.23	2.73	2.03	2
	0.0009	0.0009	0.044	0.05	0.06	0.04	0.06	0.06	0.04	0.04	
NGC2298	0.0093	0.0364	0.570	0.72	0.74	0.36	3.53	1.81	3.00	2.29	2
	0.0024	0.0024	0.100	0.12	0.13	0.10	0.16	0.16	0.11	0.10	
NGC2808	0.0256	0.0770	1.120	1.45	1.38	0.88	1.20	-0.95	1.66	0.93	2
	0.0007	0.0007	0.029	0.03	0.04	0.03	0.05	0.04	0.03	0.03	
NGC3201	0.0096	0.0550	1.029	1.12	1.07	0.77	2.50	0.32	2.35	1.52	2
	0.0014	0.0014	0.060	0.07	0.08	0.06	0.10	0.10	0.07	0.06	
NGC5286	0.0174	0.0517	0.752	0.91	0.94	0.54	3.03	1.01	2.66	1.90	2
	0.0007	0.0007	0.032	0.04	0.04	0.03	0.05	0.05	0.03	0.03	

Table 8—Continued

ID	Mg ₁ (mag)	Mg ₂ (mag)	Mgb (Å)	Fe5270 (Å)	Fe5335 (Å)	Fe5406 (Å)	Hδ _A (Å)	Hγ _A (Å)	Hδ _F (Å)	Hγ _F (Å)	Source ^a
NGC5904	0.0231	0.0680	1.050	1.22	1.20	0.73	2.68	0.59	2.58	1.71	1,2
	0.0007	0.0007	0.025	0.03	0.03	0.02	0.03	0.03	0.02	0.02	
NGC5927	0.0790	0.1965	3.280	2.44	2.32	1.50	-1.65	-4.76	0.24	-1.12	2
	0.0012	0.0012	0.052	0.06	0.06	0.05	0.13	0.11	0.09	0.07	
NGC5946	0.0266	0.0575	0.670	0.96	0.79	0.51	3.07	0.77	2.66	1.85	2
	0.0030	0.0030	0.136	0.15	0.17	0.12	0.27	0.25	0.19	0.16	
NGC5986	0.0146	0.0495	0.696	0.86	0.87	0.54	3.02	1.12	2.77	2.04	2
	0.0010	0.0020	0.063	0.07	0.08	0.06	0.10	0.10	0.07	0.06	
NGC6093	0.0148	0.0451	0.735	0.87	0.74	0.39	3.10	0.97	2.80	1.87	1
	0.0301	0.0351	1.442	1.61	1.85	1.35	2.10	2.04	1.47	1.30	
NGC6121	0.0266	0.0805	1.379	1.21	1.19	0.75	2.59	0.35	2.43	1.53	2
	0.0010	0.0010	0.056	0.06	0.07	0.05	0.09	0.09	0.06	0.06	
NGC6171	0.0421	0.1120	1.868	1.61	1.48	0.89	0.99	-1.92	1.43	0.43	1,2
	0.0021	0.0021	0.087	0.10	0.11	0.08	0.19	0.18	0.14	0.12	

Table 8—Continued

ID	Mg ₁	Mg ₂	Mgb	Fe5270	Fe5335	Fe5406	H δ_A	H γ_A	H δ_F	H γ_F	Source ^a
	(mag)	(mag)	(Å)	(Å)	(Å)	(Å)	(Å)	(Å)	(Å)	(Å)	
NGC6205	0.0138	0.0525	0.715	1.25	0.88	0.66	2.29	0.82	2.33	1.81	1
	0.0362	0.0422	1.760	1.97	2.27	1.67	2.30	2.27	1.60	1.44	
NGC6218	0.0176	0.0635	1.075	1.03	0.97	0.57	2.93	0.80	2.74	1.79	1,2
	0.0020	0.0020	0.086	0.10	0.11	0.08	0.14	0.13	0.09	0.08	
NGC6229	0.0280	0.0805	1.296	1.47	1.29	0.65	2.67	0.35	2.59	1.64	1
	0.0361	0.0421	1.743	1.94	2.23	1.64	2.36	2.33	1.64	1.48	
NGC6235	0.0266	0.0785	0.953	1.43	1.39	0.84	2.57	-0.41	2.46	1.31	2
	0.0040	0.0050	0.183	0.20	0.22	0.16	0.33	0.31	0.23	0.20	
NGC6254	0.0156	0.0515	0.672	0.93	0.91	0.51	2.52	0.27	2.33	1.53	2
	0.0010	0.0010	0.057	0.06	0.07	0.05	0.09	0.09	0.06	0.05	
NGC6266	0.0256	0.0825	1.346	1.36	1.35	0.81	1.57	-0.62	1.93	1.10	2
	0.0010	0.0010	0.034	0.04	0.04	0.03	0.06	0.06	0.04	0.04	
NGC6284	0.0316	0.0870	1.298	1.29	1.26	0.82	2.25	0.06	2.38	1.49	2
	0.0009	0.0014	0.053	0.06	0.07	0.05	0.08	0.08	0.06	0.05	

Table 8—Continued

ID	Mg ₁ (mag)	Mg ₂ (mag)	Mgb (Å)	Fe5270 (Å)	Fe5335 (Å)	Fe5406 (Å)	H δ_A (Å)	H γ_A (Å)	H δ_F (Å)	H γ_F (Å)	Source ^a
NGC6304	0.0696	0.1765	3.014	2.24	2.13	1.36	-1.40	-4.66	0.31	-1.06	1,2
	0.0020	0.0020	0.083	0.09	0.10	0.07	0.20	0.18	0.13	0.11	
NGC6316	0.0571	0.1471	2.365	1.89	1.71	1.16	-0.36	-3.59	0.77	-0.56	2
	0.0014	0.0017	0.069	0.07	0.08	0.06	0.16	0.15	0.11	0.09	
NGC6333	0.0166	0.0425	0.559	0.75	0.71	0.48	3.37	1.47	2.88	2.14	2
	0.0010	0.0020	0.069	0.08	0.09	0.06	0.11	0.11	0.08	0.07	
NGC6341	0.0085	0.0233	0.042	0.53	0.70	0.50	3.37	2.12	2.93	2.42	1
	0.0204	0.0236	0.983	1.10	1.27	0.93	1.26	1.24	0.88	0.78	
NGC6342	0.0380	0.1249	2.355	1.72	1.77	1.00	-0.31	-3.31	0.77	-0.43	1,2
	0.0024	0.0031	0.118	0.13	0.15	0.11	0.25	0.23	0.17	0.15	
NGC6352	0.0576	0.1545	2.734	1.91	2.02	1.40	-0.46	-5.43	0.79	-1.35	2
	0.0020	0.0030	0.110	0.12	0.14	0.10	0.22	0.21	0.15	0.14	
NGC6356	0.0666	0.1655	2.710	2.07	1.99	1.33	-1.01	-4.00	0.54	-0.70	1,2
	0.0010	0.0020	0.067	0.07	0.08	0.06	0.14	0.13	0.09	0.08	

Table 8—Continued

ID	Mg ₁ (mag)	Mg ₂ (mag)	Mgb (Å)	Fe5270 (Å)	Fe5335 (Å)	Fe5406 (Å)	H δ_A (Å)	H γ_A (Å)	H δ_F (Å)	H γ_F (Å)	Source ^a
NGC6362	0.0346	0.1025	1.751	1.38	1.23	0.86	1.46	-1.32	1.66	0.65	2
	0.0020	0.0020	0.087	0.10	0.11	0.08	0.14	0.14	0.10	0.09	
NGC6388	0.0516	0.1355	2.017	2.18	2.05	1.40	-0.28	-2.97	0.98	-0.01	2
	0.0010	0.0010	0.038	0.04	0.05	0.03	0.07	0.07	0.05	0.04	
NGC6441	0.0626	0.1580	2.475	2.22	2.11	1.38	-0.26	-3.15	0.96	-0.10	2
	0.0007	0.0007	0.030	0.03	0.04	0.03	0.06	0.06	0.04	0.03	
NGC6517	0.0070	0.0452	0.559	0.92	0.91	0.29	2.83	0.64	2.60	1.42	1
	0.0660	0.0767	3.138	3.49	3.99	2.93	4.03	4.19	2.85	2.64	
NGC6522	0.0416	0.0965	1.271	1.43	1.33	0.85	2.53	-0.02	2.47	1.46	2
	0.0020	0.0020	0.071	0.08	0.09	0.06	0.13	0.12	0.09	0.08	
NGC6528	0.1066	0.2434	3.654	2.92	2.80	1.99	-1.95	-5.31	0.33	-1.32	1,2
	0.0008	0.0009	0.038	0.04	0.04	0.03	0.10	0.09	0.07	0.05	
NGC6544	0.0436	0.0865	0.761	1.39	1.27	0.82	1.65	-1.12	1.48	0.63	2
	0.0020	0.0030	0.107	0.11	0.13	0.09	0.24	0.22	0.17	0.14	

Table 8—Continued

ID	Mg ₁ (mag)	Mg ₂ (mag)	Mgb (Å)	Fe5270 (Å)	Fe5335 (Å)	Fe5406 (Å)	Hδ _A (Å)	Hγ _A (Å)	Hδ _F (Å)	Hγ _F (Å)	Source ^a
NGC6553	0.0976	0.2355	3.674	2.87	2.60	1.98	-1.30	-4.88	0.32	-1.08	2
	0.0020	0.0030	0.099	0.10	0.12	0.08	0.27	0.23	0.19	0.15	
NGC6569	0.0476	0.1265	1.952	1.53	1.54	1.01	0.66	-2.24	1.11	0.18	2
	0.0030	0.0030	0.119	0.13	0.14	0.10	0.27	0.25	0.19	0.16	
NGC6624	0.0556	0.1475	2.378	2.03	1.92	1.28	-0.82	-3.78	0.64	-0.52	2
	0.0007	0.0007	0.035	0.04	0.04	0.03	0.06	0.06	0.04	0.04	
NGC6626	0.0246	0.0835	1.278	1.15	1.25	0.74	2.67	0.34	2.57	1.61	1,2
	0.0010	0.0010	0.056	0.06	0.07	0.05	0.09	0.09	0.06	0.06	
NGC6637	0.0526	0.1455	2.340	1.82	1.75	1.19	-0.55	-3.70	0.69	-0.62	2
	0.0010	0.0010	0.053	0.06	0.07	0.05	0.10	0.10	0.07	0.06	
NGC6638	0.0456	0.1235	1.835	1.69	1.61	1.10	0.69	-2.45	1.26	0.14	1,2
	0.0020	0.0020	0.080	0.09	0.10	0.07	0.16	0.15	0.11	0.09	
NGC6652	0.0294	0.1005	1.889	1.54	1.51	0.87	0.71	-2.35	1.38	0.09	2
	0.0009	0.0014	0.052	0.06	0.07	0.05	0.08	0.08	0.05	0.05	

Table 8—Continued

ID	Mg ₁ (mag)	Mg ₂ (mag)	Mgb (Å)	Fe5270 (Å)	Fe5335 (Å)	Fe5406 (Å)	Hδ _A (Å)	Hγ _A (Å)	Hδ _F (Å)	Hγ _F (Å)	Source ^a
NGC6717	0.0697	0.1395	1.621	2.33	2.09	1.39	2.95	-0.68	2.73	1.27	1
	0.0372	0.0435	1.805	1.95	2.20	1.60	2.82	2.74	1.97	1.74	
NGC6723	0.0206	0.0755	1.266	1.19	1.10	0.69	1.77	-0.62	1.94	1.09	2
	0.0020	0.0020	0.080	0.09	0.10	0.08	0.13	0.12	0.09	0.08	
NGC6752	0.0126	0.0455	0.723	0.84	0.86	0.46	3.01	1.23	2.80	2.08	2
	0.0010	0.0010	0.050	0.06	0.07	0.05	0.06	0.07	0.04	0.04	
NGC6779	0.0170	0.0410	0.443	1.00	0.54	0.32	3.53	1.83	2.97	2.39	1
	0.0794	0.0923	3.789	4.29	4.93	3.62	4.59	4.69	3.24	2.99	
NGC6838	0.0707	0.1582	2.528	2.11	1.83	1.18	0.09	-3.89	1.04	-0.83	1
	0.0736	0.0857	3.533	3.91	4.45	3.29	4.71	4.77	3.30	3.07	
NGC6864	0.0271	0.0820	1.293	1.64	1.40	0.84	2.02	-0.39	2.18	1.33	1
	0.0230	0.0269	1.109	1.22	1.40	1.02	1.69	1.62	1.18	1.03	
NGC6934	0.0140	0.0438	0.231	1.14	0.70	0.91	2.69	0.82	2.52	1.84	1
	0.0446	0.0517	2.157	2.40	2.77	2.03	2.84	2.80	1.99	1.78	

Table 8—Continued

ID	Mg ₁ (mag)	Mg ₂ (mag)	Mgb (Å)	Fe5270 (Å)	Fe5335 (Å)	Fe5406 (Å)	Hδ _A (Å)	Hγ _A (Å)	Hδ _F (Å)	Hγ _F (Å)	Source ^a
NGC6981	0.0273	0.0698	1.102	1.10	1.22	0.63	3.15	0.64	2.80	1.73	1
	0.0851	0.0990	4.090	4.63	5.34	3.93	4.85	4.96	3.42	3.16	
NGC7006	0.0133	0.0448	0.121	0.91	0.67	0.77	2.51	0.51	2.46	1.76	1
	0.0714	0.0830	3.466	3.88	4.48	3.29	4.18	4.24	2.94	2.70	
NGC7078	0.0101	0.0287	0.353	0.43	0.53	0.25	3.81	2.53	3.15	2.61	1,2
	0.0007	0.0009	0.037	0.04	0.05	0.04	0.05	0.05	0.03	0.03	
NGC7089	0.0156	0.0495	0.727	0.95	0.94	0.57	3.08	1.14	2.76	2.02	1,2
	0.0010	0.0010	0.058	0.07	0.08	0.06	0.08	0.08	0.05	0.05	

Note. — (a) Sources of LIS indices: 1 = this work; 2 = SRC05

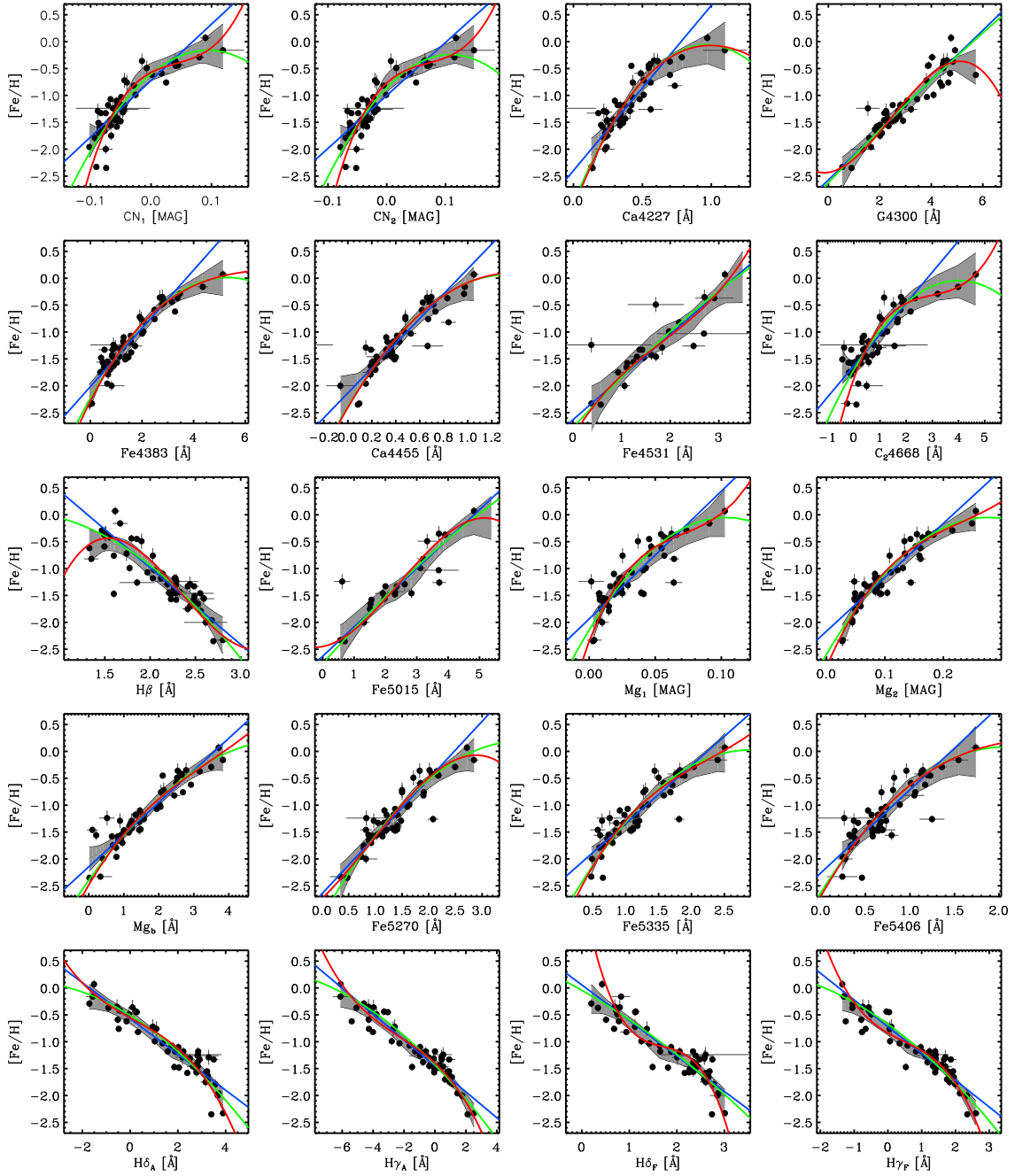


Fig. 9.— The Lick/S07 index–metallicity relations. The blue, green, and red solid lines represent the first-, second-, and third-order orthogonal least-squares fit, respectively. The gray-shaded regions indicate the 95% confidence bands based on the LOESS regression, which show the underlying trend of the data.

Table 9. Coefficients of the Lick/S07 index versus metallicity relations. The coefficients were obtained by the orthogonal distance least-squares fit of a linear function $[\text{Fe}/\text{H}] = a_0 + a_1 \times (\text{index})$ to 53 GGC data.

Index	a_0	a_1	BIC ^a	Valid Range
CN ₁ [mag]	-0.7236 ± 0.0414	10.4914 ± 0.6798	59.5	[-1.4887, 2.4745]
CN ₂ [mag]	-1.0003 ± 0.0319	9.8522 ± 0.6217	53.1	[-2.0814, 3.0346]
Ca4227 [Å]	-2.3964 ± 0.0908	3.0696 ± 0.2045	71.4	[-2.08, 3.03]
G4300 [Å]	-2.5737 ± 0.0670	0.4640 ± 0.0208	27.7	[-1.49, 2.45]
Fe4383 [Å]	-2.0139 ± 0.0508	0.5412 ± 0.0274	31.5	[-2.08, 3.02]
Ca4455 [Å]	-2.1353 ± 0.0546	2.3100 ± 0.1115	44.1	[-2.08, 3.02]
Fe4531 [Å]	-2.6327 ± 0.0872	0.7934 ± 0.0417	14.4	[-2.12, 2.75]
C ₂ 4668 [Å]	-1.6293 ± 0.0532	0.5806 ± 0.0439	66.9	[-2.12, 3.38]
H β [Å]	1.8738 ± 0.1863	-1.4286 ± 0.0869	68.0	[-2.12, 3.38]
Fe5015 [Å]	-2.6300 ± 0.0956	0.5446 ± 0.0309	20.0	[-2.12, 1.82]
Mg ₁ [mag]	-1.9366 ± 0.2901	23.7475 ± 1.4533	65.5	[-2.1173, 1.8161]
Mg ₂ [mag]	-2.1661 ± 0.0577	10.0347 ± 0.5045	34.2	[-2.1173, 2.2734]
Mgb [Å]	-2.1445 ± 0.0437	0.5969 ± 0.0239	18.7	[-2.117, 1.673]
Fe5270 [Å]	-2.6468 ± 0.0754	1.0683 ± 0.0504	39.6	[-2.12, 3.18]
Fe5335 [Å]	-2.4219 ± 0.0699	1.0807 ± 0.0549	42.3	[-2.12, 3.18]
Fe5406 [Å]	-2.2595 ± 0.0751	1.5459 ± 0.0934	62.6	[-2.12, 2.47]

Table 9—Continued

Index	a_0	a_1	BIC ^a	Valid Range
H δ_A [Å]	-0.5677 ± 0.0346	-0.3335 ± 0.0146	24.1	[-2.12, 2.47]
H δ_F [Å]	-1.4494 ± 0.0245	-0.2412 ± 0.0096	19.1	[-2.12, 2.47]
H γ_A [Å]	0.0567 ± 0.0695	-0.6601 ± 0.0345	46.9	[-1.92, 1.93]
H γ_F [Å]	-0.7204 ± 0.0284	-0.4980 ± 0.0208	23.5	[-1.92, 1.93]

^aBIC=Bayesian information criterion

Table 10. The same as Table 9, but using a quadratic polynomial $[\text{Fe}/\text{H}] = a_0 + a_1 \times (\text{index}) + a_2 \times (\text{index})^2$ to the 53 GGC data.

Index	a_0	a_1	a_2	BIC ^a	Valid Range
CN ₁ [mag]	-0.6024 ± 0.0581	9.3732 ± 1.2557	-49.7232 ± 10.6338	57.1	[-1.4887, 2.4745]
CN ₂ [mag]	-0.8565 ± 0.0431	11.3391 ± 0.9451	-52.1753 ± 9.9137	53.4	[-2.0814, 3.0346]
Ca4227 [Å]	-2.9955 ± 0.1258	6.0801 ± 0.4681	-3.1461 ± 0.5158	56.1	[-2.08, 3.03]
G4300 [Å]	-2.6238 ± 0.1798	0.5025 ± 0.1115	-0.0064 ± 0.0182	30.9	[-1.49, 2.45]
Fe4383 [Å]	-2.2307 ± 0.0616	0.8459 ± 0.0512	-0.0797 ± 0.0137	24.7	[-2.08, 3.02]
Ca4455 [Å]	-2.3949 ± 0.0909	3.7176 ± 0.3328	-1.4066 ± 0.3642	44.3	[-2.08, 3.02]
Fe4531 [Å]	-2.7763 ± 0.1760	0.9818 ± 0.1679	-0.0453 ± 0.0427	5.4	[-2.12, 2.75]
C ₂ 4668 [Å]	-1.7058 ± 0.0550	0.8308 ± 0.0549	-0.1038 ± 0.0187	52.1	[-2.12, 3.38]
H β [Å]	-0.0173 ± 1.0020	0.3868 ± 0.9390	-0.4241 ± 0.2220	60.7	[-2.12, 3.38]
Fe5015 [Å]	-2.7707 ± 0.2046	0.6659 ± 0.1292	-0.0215 ± 0.0220	21.6	[-2.12, 1.82]
Mg ₁ [mag]	-2.1407 ± 0.0881	40.4836 ± 3.6554	-195.7725 ± 49.4459	64.7	[-2.1173, 1.8161]
Mg ₂ [mag]	-2.5950 ± 0.0935	18.3873 ± 1.4463	-33.1914 ± 6.5331	32.4	[-2.1173, 2.2734]
Mgb [Å]	-2.3957 ± 0.0765	0.9159 ± 0.0765	-0.0801 ± 0.0224	17.7	[-2.117, 1.673]
Fe5270 [Å]	-3.0791 ± 0.1524	1.7413 ± 0.1925	-0.2314 ± 0.0660	42.8	[-2.12, 3.18]
Fe5335 [Å]	-3.1173 ± 0.1699	2.1828 ± 0.2533	-0.3792 ± 0.1035	54.7	[-2.12, 3.18]
Fe5406 [Å]	-2.6258 ± 0.1357	2.6388 ± 0.3101	-0.6436 ± 0.2015	57.0	[-2.12, 2.47]

Table 10—Continued

Index	a_0	a_1	a_2	BIC ^a	Valid Range
H δ_A [Å]	-0.5101 ± 0.0575	-0.2767 ± 0.0413	-0.0295 ± 0.0102	26.0	[-2.12, 2.47]
H δ_F [Å]	-1.4287 ± 0.0317	-0.2955 ± 0.0140	-0.0120 ± 0.0040	11.6	[-2.12, 2.47]
H γ_A [Å]	-0.0434 ± 0.2065	-0.5011 ± 0.2071	-0.0479 ± 0.0552	49.6	[-1.92, 1.93]
H γ_F [Å]	-0.6733 ± 0.0441	-0.4522 ± 0.0444	-0.0492 ± 0.0225	29.7	[-1.92, 1.93]

^aBIC=Bayesian information criterion

Table 11. The same as Table 9, but using a cubic polynomial

$$[\text{Fe}/\text{H}] = a_0 + a_1 \times (\text{index}) + a_2 \times (\text{index})^2 + a_3 \times (\text{index})^3 \text{ to the 53 GGC data.}$$

Index	a_0	a_1	a_2	a_3	BIC ^a	Valid Range
CN ₁ [mag]	-0.5734 ± 0.0853	5.8757 ± 2.5474	-67.1465 ± 34.7753	544.9103 ± 192.8483	78.0	[-1.4887, 2.4745]
CN ₂ [mag]	-0.7675 ± 0.0583	9.9262 ± 1.3624	-101.2412 ± 25.4773	487.9831 ± 171.5745	74.9	[-2.0814, 3.0346]
Ca4227 [Å]	-3.0963 ± 0.2829	6.7401 ± 1.5366	-4.3666 ± 2.9654	0.6519 ± 2.1818	60.7	[-2.08, 3.03]
G4300 [Å]	-2.4314 ± 0.3315	0.0733 ± 0.2901	0.2073 ± 0.0911	-0.0279 ± 0.0099	38.6	[-1.49, 2.45]
Fe4383 [Å]	-2.2833 ± 0.1023	0.9469 ± 0.1205	-0.1265 ± 0.0537	0.0059 ± 0.0095	29.5	[-2.08, 3.02]
Ca4455 [Å]	-2.4062 ± 0.1502	3.8081 ± 0.7475	-1.5953 ± 1.4999	0.1113 ± 1.1220	48.8	[-2.08, 3.02]
Fe4531 [Å]	-2.9404 ± 0.5046	1.4908 ± 0.6961	-0.4374 ± 0.3443	0.0800 ± 0.0588	24.4	[-2.12, 2.75]
C ₂ 4668 [Å]	-1.8760 ± 0.1041	1.3531 ± 0.1605	-0.4178 ± 0.0986	0.0467 ± 0.0223	87.3	[-2.12, 3.38]
H β [Å]	-9.6428 ± 5.6060	14.2790 ± 7.8815	-6.8978 ± 3.7163	0.9792 ± 0.5867	72.4	[-2.12, 3.38]
Fe5015 [Å]	-2.4500 ± 0.3844	0.1127 ± 0.3510	0.2259 ± 0.1168	-0.0306 ± 0.0135	16.2	[-2.12, 1.82]
Mg ₁ [mag]	-2.3518 ± 0.1425	64.4501 ± 8.5221	-767.6376 ± 189.8145	3602.3560 ± 1666.7000	57.7	[-2.1173, 1.8161]
Mg ₂ [mag]	-2.8326 ± 0.1960	25.3661 ± 4.3207	-89.3218 ± 34.6858	130.0747 ± 104.0610	34.3	[-2.1173, 2.2734]
Mgb [Å]	-2.4818 ± 0.1323	1.1074 ± 0.1839	-0.1923 ± 0.0989	0.0186 ± 0.0196	21.6	[-2.117, 1.673]
Fe5270 [Å]	-2.7353 ± 0.3229	0.9577 ± 0.5885	0.2963 ± 0.3884	-0.1068 ± 0.0899	45.8	[-2.12, 3.18]
Fe5335 [Å]	-3.3910 ± 0.4238	2.9746 ± 0.9065	-1.0225 ± 0.6936	0.1513 ± 0.1895	62.4	[-2.12, 3.18]
Fe5406 [Å]	-2.6922 ± 0.2859	2.9066 ± 0.9243	-0.9495 ± 1.0935	0.1027 ± 0.4745	61.3	[-2.12, 2.47]

Table 11—Continued

Index	a_0	a_1	a_2	a_3	BIC ^a	Valid Range
H δ_A [Å]	-0.5536 ± 0.0977	-0.2468 ± 0.0976	0.0095 ± 0.0413	-0.0147 ± 0.0069	37.3	[-2.12, 2.47]
H δ_F [Å]	-1.3986 ± 0.0382	-0.2684 ± 0.0225	-0.0360 ± 0.0077	-0.0053 ± 0.0016	19.1	[-2.12, 2.47]
H γ_A [Å]	1.8203 ± 0.7955	-4.6664 ± 1.1832	2.5960 ± 0.6178	-0.5046 ± 0.1106	84.7	[-1.92, 1.93]
H γ_F [Å]	-0.8384 ± 0.0525	-0.3629 ± 0.0682	0.1204 ± 0.0495	-0.0856 ± 0.0178	19.0	[-1.92, 1.93]

^aBIC=Bayesian information criterion

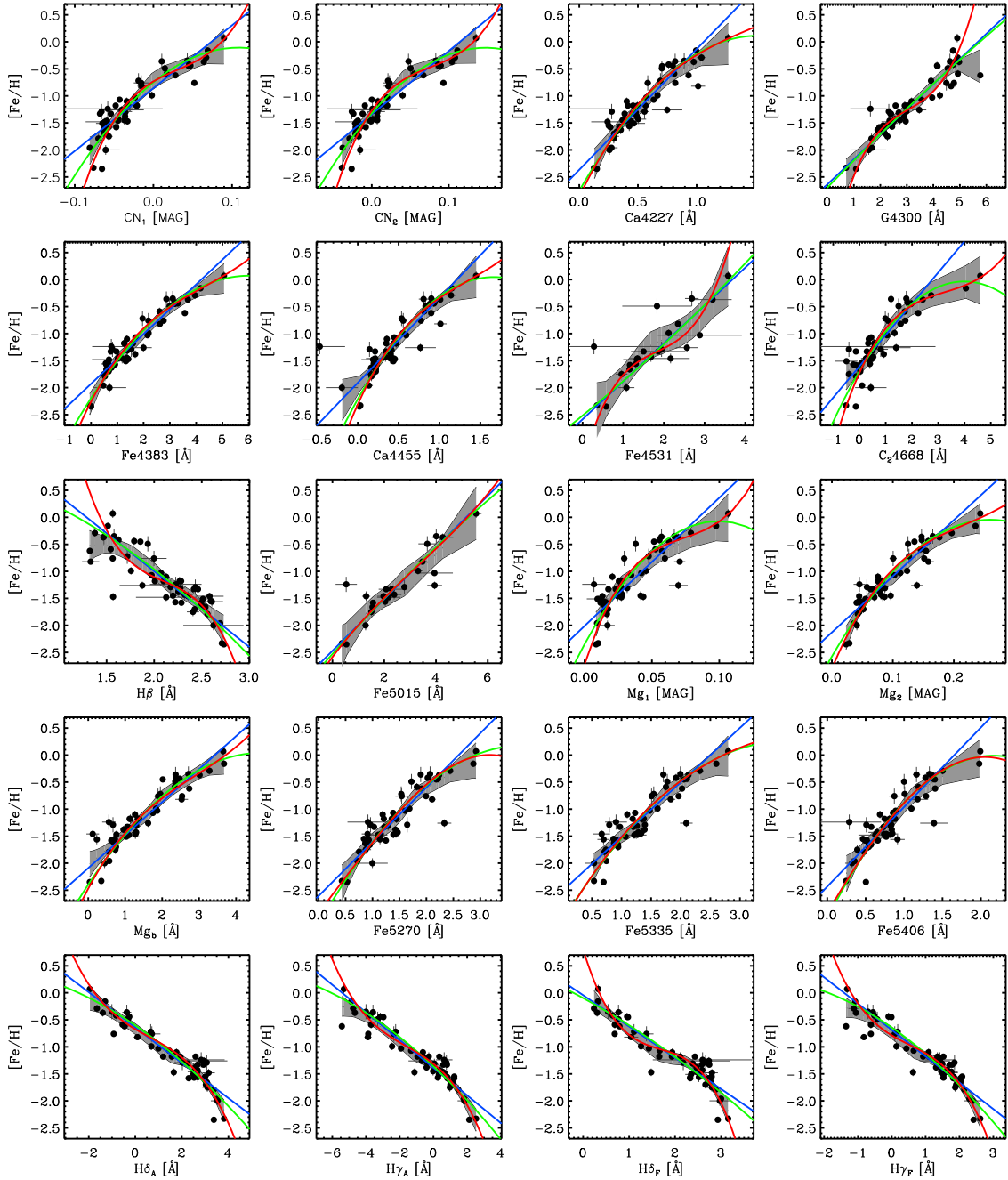


Fig. 10.— The LIS index–metallicity relations. The blue, green, and red solid lines represent the first-, second-, and third-order orthogonal least-squares fit, respectively. The gray-shaded regions indicate the 95% confidence bands based on the LOESS regression, which show the underlying trend of the data.

Table 12. Coefficients of the LIS index versus metallicity relations. The coefficients were obtained by the orthogonal distance least-squares fit of a linear function $[\text{Fe}/\text{H}] = a_0 + a_1 \times (\text{index})$ to 53 GGC data.

Index	a_0	a_1	BIC ^a	Valid Range
CN ₁ [mag]	-0.8572 ± 0.0293	11.6263 ± 0.5863	38.1	[-1.4887, 2.5112]
CN ₂ [mag]	-1.3408 ± 0.0290	11.7227 ± 0.6203	42.8	[-2.0814, 2.5112]
Ca4227 [Å]	-2.3670 ± 0.0660	2.2327 ± 0.1102	46.3	[-2.12, 2.51]
G4300 [Å]	-2.6373 ± 0.0689	0.4643 ± 0.0205	29.6	[-1.49, 2.62]
Fe4383 [Å]	-1.9284 ± 0.0398	0.4596 ± 0.0199	12.4	[-2.08, 2.62]
Ca4455 [Å]	-1.9097 ± 0.0404	1.5739 ± 0.0684	23.0	[-2.12, 2.62]
Fe4531 [Å]	-2.5856 ± 0.1207	0.7018 ± 0.0608	25.8	[-2.12, 2.78]
C ₂ 4668 [Å]	-1.6046 ± 0.0467	0.5787 ± 0.0395	57.0	[-2.12, 2.78]
H β [Å]	1.8098 ± 0.1826	-1.4028 ± 0.0854	68.1	[-2.12, 2.78]
Fe5015 [Å]	-2.4702 ± 0.0859	0.4782 ± 0.0301	14.5	[-2.12, 1.82]
Mg ₁ [mag]	-2.0109 ± 0.0679	23.7311 ± 1.5929	76.6	[-2.1173, 1.8161]
Mg ₂ [mag]	-2.1295 ± 0.0572	10.3913 ± 0.5326	36.0	[-2.1173, 2.2293]
Mgb [Å]	-2.0913 ± 0.0446	0.6104 ± 0.0260	24.3	[-1.417, 2.081]
Fe5270 [Å]	-2.6073 ± 0.0831	1.0038 ± 0.0535	56.1	[-2.12, 2.85]
Fe5335 [Å]	-2.5166 ± 0.0761	1.0068 ± 0.0520	47.0	[-2.12, 2.85]
Fe5406 [Å]	-2.4342 ± 0.0791	1.4730 ± 0.0828	51.4	[-1.97, 2.78]

Table 12—Continued

Index	a_0	a_1	BIC ^a	Valid Range
H δ_A [Å]	-0.6419 ± 0.0270	-0.3268 ± 0.0120	7.4	[-2.12, 2.78]
H δ_F [Å]	-1.3868 ± 0.0234	-0.2560 ± 0.0102	19.6	[-2.12, 2.78]
H γ_A [Å]	-0.0443 ± 0.0520	-0.5786 ± 0.0247	21.5	[-1.74, 2.20]
H γ_F [Å]	-0.6878 ± 0.0281	-0.4879 ± 0.0196	19.9	[-1.74, 2.20]

^aBIC=Bayesian information criterion

Table 13. The same as Table 9, but using a quadratic polynomial $[\text{Fe}/\text{H}] = a_0 + a_1 \times (\text{index}) + a_2 \times (\text{index})^2$ to the 53 GGC data.

Index	a_0	a_1	a_2	BIC ^a	Valid Range
CN ₁ [mag]	-0.7465 ± 0.0408	11.8023 ± 1.0299	-54.4875 ± 13.3298	33.7	[-1.4887, 2.5112]
CN ₂ [mag]	-1.3196 ± 0.0392	16.3757 ± 0.9635	-55.4078 ± 13.4646	39.8	[-2.0814, 2.5112]
Ca4227 [Å]	-2.7543 ± 0.1225	3.7625 ± 0.3828	-1.2343 ± 0.3356	41.0	[-2.12, 2.51]
G4300 [Å]	-2.6957 ± 0.2014	0.5063 ± 0.1202	-0.0066 ± 0.0187	32.7	[-1.49, 2.62]
Fe4383 [Å]	-2.1948 ± 0.0608	0.7540 ± 0.0505	-0.0627 ± 0.0133	18.9	[-2.08, 2.62]
Ca4455 [Å]	-2.2119 ± 0.0688	2.7134 ± 0.2019	-0.8150 ± 0.1859	27.3	[-2.12, 2.62]
Fe4531 [Å]	-2.5163 ± 0.2575	0.6147 ± 0.2505	0.0224 ± 0.0671	28.9	[-2.12, 2.78]
C ₂ 4668 [Å]	-1.6931 ± 0.0517	0.8317 ± 0.0511	-0.1043 ± 0.0180	53.6	[-2.12, 2.78]
H β [Å]	0.8764 ± 1.0545	-0.4646 ± 0.9915	-0.2271 ± 0.2352	69.9	[-2.12, 2.78]
Fe5015 [Å]	-2.5288 ± 0.1617	0.5326 ± 0.1066	-0.0098 ± 0.0200	17.2	[-2.12, 1.82]
Mg ₁ [mag]	-2.3471 ± 0.1042	45.8900 ± 4.0885	-231.2786 ± 50.4986	66.7	[-2.1173, 1.8161]
Mg ₂ [mag]	-2.5747 ± 0.0976	19.4831 ± 1.5965	-37.5029 ± 7.6911	40.0	[-2.1173, 2.2293]
Mgb [Å]	-2.3972 ± 0.0774	1.0385 ± 0.0814	-0.1105 ± 0.0256	24.1	[-1.417, 2.081]
Fe5270 [Å]	-3.1278 ± 0.1785	1.7447 ± 0.2194	-0.2301 ± 0.0730	55.8	[-2.12, 2.85]
Fe5335 [Å]	-3.0688 ± 0.1798	1.7645 ± 0.2362	-0.2341 ± 0.0838	53.7	[-2.12, 2.85]
Fe5406 [Å]	-3.0224 ± 0.1559	2.7839 ± 0.2954	-0.6432 ± 0.1574	66.3	[-1.97, 2.78]

Table 13—Continued

Index	a_0	a_1	a_2	BIC ^a	Valid Range
H δ_A [Å]	-0.6032 ± 0.0476	-0.2951 ± 0.0344	-0.0197 ± 0.0096	18.6	[-2.12, 2.78]
H δ_F [Å]	-1.3594 ± 0.0346	-0.2932 ± 0.0150	-0.0114 ± 0.0053	20.3	[-2.12, 2.78]
H γ_A [Å]	-0.0970 ± 0.1698	-0.4645 ± 0.1633	-0.0396 ± 0.0420	34.0	[-1.74, 2.20]
H γ_F [Å]	-0.6413 ± 0.0457	-0.4346 ± 0.0463	-0.0497 ± 0.0221	26.6	[-1.74, 2.20]

^aBIC=Bayesian information criterion

Table 14. The same as Table 9, but using a cubic polynomial

$$[\text{Fe}/\text{H}] = a_0 + a_1 \times (\text{index}) + a_2 \times (\text{index})^2 + a_3 \times (\text{index})^3 \text{ to the 53 GGC data.}$$

Index	a_0	a_1	a_2	a_3	BIC ^a	Valid Range
CN ₁ [mag]	-0.7321 ± 0.0566	8.5305 ± 1.9158	-76.9963 ± 36.2398	871.5720 ± 328.5897	51.4	[-1.4887, 2.5112]
CN ₂ [mag]	-1.2693 ± 0.0504	20.4390 ± 1.5696	-196.3766 ± 30.7768	865.7252 ± 300.5097	50.7	[-2.0814, 2.5112]
Ca4227 [Å]	-2.8616 ± 0.2526	4.4588 ± 1.1041	-2.3699 ± 1.7731	0.5285 ± 1.0364	52.2	[-2.12, 2.51]
G4300 [Å]	-4.2812 ± 0.6967	2.4309 ± 0.6108	-0.7105 ± 0.1865	0.0783 ± 0.0194	54.3	[-1.49, 2.62]
Fe4383 [Å]	-2.2594 ± 0.1013	0.9426 ± 0.1160	-0.1558 ± 0.0517	0.0120 ± 0.0090	26.6	[-2.08, 2.62]
Ca4455 [Å]	-2.3102 ± 0.1116	3.3596 ± 0.4524	-1.8492 ± 0.7002	0.4571 ± 0.4229	31.2	[-2.12, 2.62]
Fe4531 [Å]	-3.4107 ± 0.5701	2.6925 ± 0.7989	-1.2758 ± 0.4152	0.2322 ± 0.0754	33.9	[-2.12, 2.78]
C ₂ 4668 [Å]	-1.7261 ± 0.0739	1.0741 ± 0.1088	-0.2826 ± 0.0682	0.0288 ± 0.0159	62.6	[-2.12, 2.78]
H β [Å]	21.2279 ± 7.3353	-30.4620 ± 10.3598	14.1288 ± 4.9046	-2.2404 ± 0.7771	88.9	[-2.12, 2.78]
Fe5015 [Å]	-2.5846 ± 0.2998	0.6382 ± 0.2753	-0.0579 ± 0.0973	0.0059 ± 0.0123	20.0	[-2.12, 1.82]
Mg ₁ [mag]	-2.7239 ± 0.2112	78.5716 ± 12.1470	-954.2826 ± 252.9314	4329.9048 ± 2049.7900	76.3	[-2.1173, 1.8161]
Mg ₂ [mag]	-2.7992 ± 0.1953	26.8905 ± 4.5576	-100.7226 ± 38.8622	153.4423 ± 124.4089	37.4	[-2.1173, 2.2293]
Mgb [Å]	-2.4712 ± 0.1450	1.2874 ± 0.2147	-0.2931 ± 0.1216	0.0338 ± 0.0258	33.4	[-1.417, 2.081]
Fe5270 [Å]	-2.9184 ± 0.3987	1.3010 ± 0.7066	0.0500 ± 0.4502	-0.0535 ± 0.1008	59.5	[-2.12, 2.85]
Fe5335 [Å]	-3.1049 ± 0.4557	1.8942 ± 0.8642	-0.3297 ± 0.5849	0.0195 ± 0.1392	63.8	[-2.12, 2.85]
Fe5406 [Å]	-2.9303 ± 0.3367	2.4833 ± 0.9099	-0.3578 ± 0.8967	-0.0804 ± 0.3212	69.4	[-1.97, 2.78]

Table 14—Continued

Index	a_0	a_1	a_2	a_3	BIC ^a	Valid Range
H δ_A [Å]	-0.6726 ± 0.0748	-0.2556 ± 0.0735	0.0381 ± 0.0337	-0.0208 ± 0.0064	30.7	[-2.12, 2.78]
H δ_F [Å]	-1.3139 ± 0.0390	-0.2517 ± 0.0249	-0.0464 ± 0.0089	-0.0097 ± 0.0023	24.1	[-2.12, 2.78]
H γ_A [Å]	0.8068 ± 0.4878	-2.7863 ± 0.6833	1.5002 ± 0.3394	-0.2959 ± 0.0584	55.6	[-1.74, 2.20]
H γ_F [Å]	-0.7876 ± 0.0560	-0.3791 ± 0.0741	0.1298 ± 0.0534	-0.0822 ± 0.0177	19.0	[-1.74, 2.20]

^aBIC=Bayesian information criterion